

4D Millimeter-Wave Radar in Autonomous Driving: A Survey

Zeyu Han¹, Jiahao Wang¹, Zikun Xu¹, Shuocheng Yang², Lei He¹, Shaobing Xu¹, Jianqiang Wang^{1,*}, Keqiang Li^{1,*}

Abstract—The 4D millimeter-wave (mmWave) radar, proficient in measuring the range, azimuth, elevation, and velocity of targets, has attracted considerable interest within the autonomous driving community. This is attributed to its robustness in extreme environments and the velocity and elevation measurement capabilities. However, despite the rapid advancement in research related to its sensing theory and application, there is a conspicuous absence of comprehensive surveys on the subject of 4D mmWave radar. In an effort to bridge this gap and stimulate future research, this paper presents an exhaustive survey on the utilization of 4D mmWave radar in autonomous driving. Initially, the paper provides reviews on the theoretical background and progress of 4D mmWave radars, encompassing aspects such as the signal processing workflow, resolution improvement approaches, and extrinsic calibration process. Learning-based radar data quality improvement methods are present following. Then, this paper introduces relevant datasets and application algorithms in autonomous driving perception, localization and mapping tasks. Finally, this paper concludes by forecasting future trends in the realm of 4D mmWave radar in autonomous driving. To the best of our knowledge, this is the first survey specifically dedicated to the 4D mmWave radar in autonomous driving.

I. INTRODUCTION

Autonomous driving technology, which aspires to provide safe, convenient, and comfortable transportation experiences, is advancing at a remarkable pace. To realize high-level autonomous driving, the capabilities of environment perception, localization and mapping are indispensable. Consequently, the sensors deployed on autonomous vehicles, such as cameras, LiDARs, and radars, along with their application algorithms, are garnering increasing research interest.

Among the various sensors, mmWave radars, with their acknowledged advantages of compact size, cost-effectiveness, all-weather adaptation, velocity-measuring capability, and long detection range, etc. [1], have always been extensively employed in autonomous driving. However, conventional mmWave radars, often referred to as 3D mmWave radars, demonstrate limited efficacy in measuring the elevation of targets, and their data typically encompassing only range, azimuth, and Doppler velocity information. Additionally, 3D mmWave radars suffer from clutter, noise, and low resolution, particularly in the angular dimension. These limitations further constrain their suitability for intricate perception tasks.

The recent advancement of multiple-input multiple-output (MIMO) antenna technology has catalyzed a significant en-

Zeyu Han and Jiahao Wang contribute equally to this work.

This work was supported by the National Natural Science Foundation of China (NSFC) under grant number 52221005 and Tsinghua University - Chongqing Changan Automobile Co., Ltd. Joint Research Project.

¹School of Vehicle and Mobility, Tsinghua University, Beijing, China

²Xingjian College, Tsinghua University, Beijing, China

*Correspondence: wjqlws@tsinghua.edu.cn (J.W.), likq@tsinghua.edu.cn (K.L.)

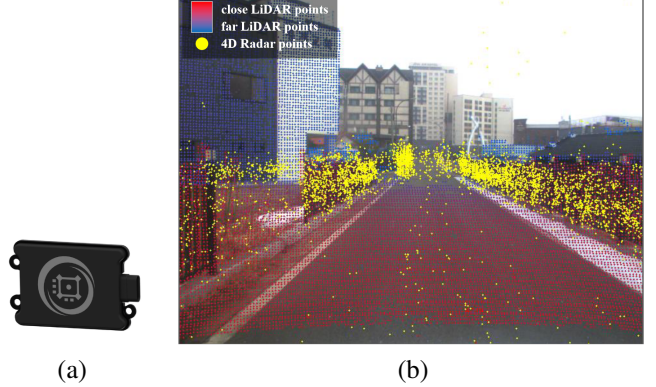


Fig. 1. The Oculii Eagle 4D mmWave radar (a) and its point cloud comparing with the Ouster 128-channel LiDAR (b) [2], [3]

hancement in elevational resolution, leading to the emergence of 4D mmWave radars. As the name suggests, 4D mmWave radars are capable of measuring four distinct types of target information: range, azimuth, elevation, and velocity. In addition to the augmented elevational resolution, 4D mmWave radars still preserve the salient advantages of their 3D predecessors. Enterprises that involve in the 4D mmWave radar industry ranging from conventional suppliers like Bosch, Continental, and ZF, to a host of burgeoning tech companies such as Arbe, Huawei, and Oculii. An illustrative example of this technology is the Oculii Eagle 4D mmWave radar, which, when juxtaposed with the Ouster 128-channel LiDAR, demonstrates its capabilities such as long detection range through the point cloud representation as depicted in Fig. 1.

The 4D mmWave radar not only represents an improved version of mmWave radars but also ushers in a multitude of significant research avenues. The raw data volume generated by 4D mmWave radars substantially exceeds that of their traditional counterparts, thereby presenting formidable challenges in signal processing and data generation, particularly in the presence of clutter and noise. The sparsity and noise inherent in 4D mmWave radar point clouds, generated in the existing signal processing workflow are markedly more severe than those in LiDAR point clouds. This necessitates the careful design of perception, localization and mapping algorithms that duly accommodate the intrinsic characteristics of the 4D mmWave radar.

Numerous surveys have been conducted on the theory and application of mmWave radars. In recent years, Bilik et al. [4] have reviewed the challenges faced by mmWave radars in autonomous driving and its future trends. Venon et al. [5] have provided a comprehensive summary of the theory and existing perception algorithms of mmWave radar in autonomous driving, while Harlow et al. [6] have concentrated

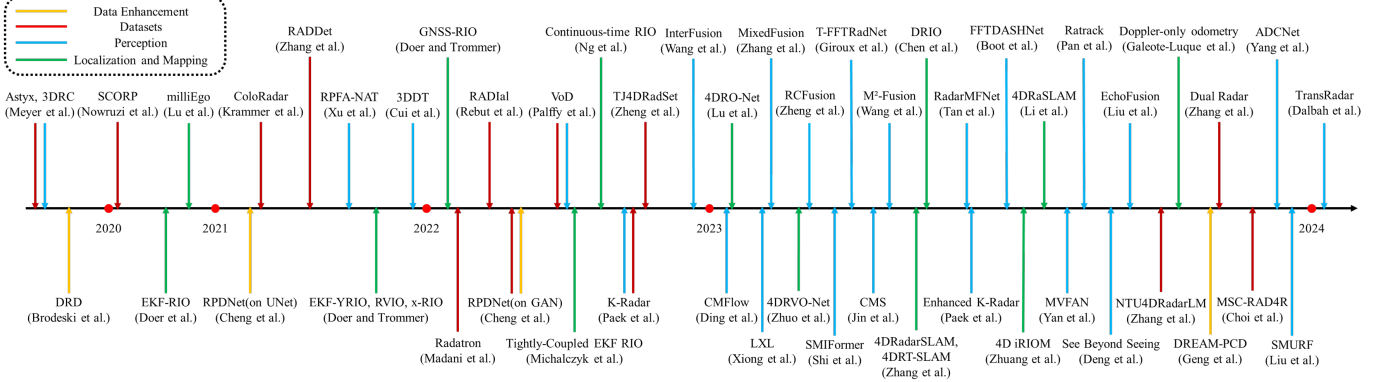


Fig. 2. The timeline of 4D mmWave radar datasets, learning-based radar data quality improvement methods, and perception, localization and mapping algorithms

on mmWave radar applications in robotics for their survey. It is evident that most reviews are centered on 3D mmWave radars.

Despite the transformative emergence of 4D mmWave radars and associated algorithms, there have been few specialized surveys. To bridge this gap, this paper presents a thorough review of 4D mmWave radars in autonomous driving. The principal contributions of this work can be summarized as follows:

- To the best of our knowledge, this is the first survey concentrating on 4D mmWave radars within the context of autonomous driving.
- Acknowledging the distinctiveness of 4D mmWave radars, this survey delineates its theoretical background, signal processing workflow, and discusses newly emerged learning-based radar data quality improvement methods.
- This paper delivers an extensive survey of 4D mmWave radar application algorithms in autonomous driving. It systematically presents related datasets, as well as research on perception, localization and mapping algorithms of 4D mmWave radars, all of which are chronologically depicted on a timeline in Fig. 2.

The remainder of this paper is organized as follows: Section II introduces the foundational theory of 4D mmWave radars, including the signal processing workflow, data formats, and the methods for improving resolution and calibration. Following Sections illustrate newly evolved 4D mmWave radar technologies in autonomous driving, as categorised in Fig. 3. Section III lists available 4D mmWave radar datasets for researchers' convenience. Section IV summarizes some learning-based methods for radar data quality improvement. Section V reviews 4D mmWave radar perception applications, categorized into different input formats. Moreover, 4D mmWave radar applications in localization and mapping are presented in Section VI. Section VII discusses future trends of 4D mmWave radar in autonomous driving, and Section VIII draws the conclusion.

II. BACKGROUND OF 4D MMWAVE RADARS

For researchers dedicated to the field of autonomous driving, fundamental knowledge about 4D mmWave radars may often be undervalued. This section briefly revisits the basic theory of

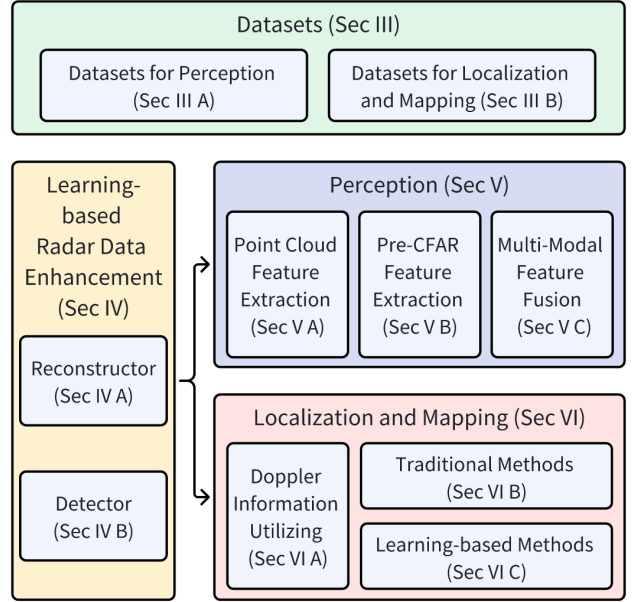


Fig. 3. The categories of newly evolved 4D mmWave radar technologies in autonomous driving.

4D mmWave radars, laying the groundwork for the subsequent discussions.

A. Signal Processing Workflow

The traditional signal processing workflow and corresponding data formats of 4D mmWave radars are shown in Fig.4. In step 1, millimeter waves are transmitted from the transmitting (TX) antennas. These waves, upon encountering surrounding targets, are reflected back to receiving (RX) antennas. The waveform employed by the majority of extant 4D mmWave radars is the Frequency Modulated Continuous Wave (FMCW), which is renowned for its superior resolution capabilities in comparison to alternative waveforms. During each operational cycle (commonly referred to as a 'chirp') of the FMCW radar's TX antennas, the frequency of the emitted signal increases linearly, characterized by an initial frequency

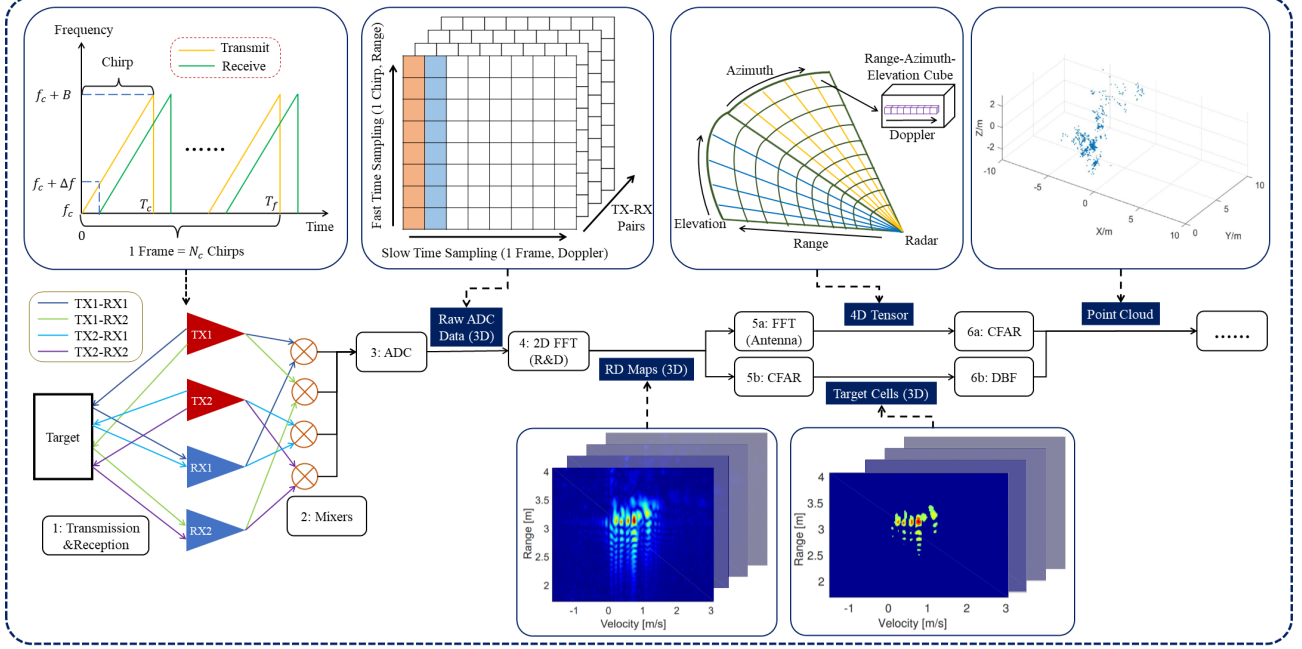


Fig. 4. The traditional signal processing workflow and corresponding data formats of 4D mmWave radars [7] [8]

f_c , a bandwidth B , a frequency slope S , and a time duration T_c . By measuring the frequency of the signal received, the range r of the target can be calculated as follows:

$$r = \frac{ct}{2}, \quad t = \frac{\Delta f}{S}, \quad (1)$$

where t denotes the temporal interval between transmission and reception, c represents the light speed, and Δf is the discrepancy in frequency between the transmitted and received signals. Concurrently, a single frame of an FMCW radar comprises N_c chirps and spans a temporal duration T_f . To avoid interference amongst successive chirps, the transmitted and received signals are considered within an individual chirp. Consequently, the maximum unambiguous range detectable by 4D mmWave radars is restricted by the chirp duration T_c . By way of illustration, the AWR1843 from Texas Instruments features a chirp duration of $T_c = 0.33\mu s$, accordingly its maximum unambiguous range is 50 meters. Presuming the target's range remains invariant within a single frame, the frequency shift between two successive chirps is employed to deduce the radial relative velocity v of the target, utilizing the Doppler effect, as delineated below:

$$v = \frac{c\Delta f}{2f_c}, \quad \Delta f = \frac{\Delta\varphi}{2\pi T_c}, \quad (2)$$

where the first equation is the Doppler effect formula, Δf and $\Delta\varphi$ correspond to the frequency and phase shifts, respectively, between the received signals of two successive chirps. It is manifest that the range and Doppler resolutions depend on parameters such as f_c, T_c, N_c . For an in-depth exposition of these dependencies, readers are directed to consult the work of Venon et al. [5].

The signals of each TX-RX pair are mixed by a mixer at step 2 and subsequently transduced into digital form by an Analog-

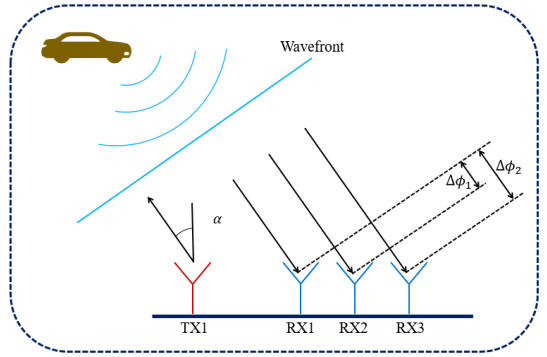


Fig. 5. The DOA estimation principle of 4D mmWave radars

to-Digital Converter (ADC) at step 3, yielding raw ADC data. It should be noted that within the matrices of raw ADC data depicted in Fig. 4, the coordinate axes represent the sampling timestamps within a chirp and a frame, respectively, while the value of each matrix element corresponds to the intensity of the reflected signal. Sampling within a chirp aims to calculate range information, and is also referred to as fast time sampling. Conversely, sampling within a frame is intended to deduce Doppler information, and is thus termed slow time sampling. Subsequently, at step 4, a two-dimensional Fast Fourier Transformation (FFT) is applied along the range and Doppler dimensions to construct the Range-Doppler (RD) map, the axes of which are range and Doppler velocity.

However, despite the RD map providing the signal intensities of different ranges and velocities, it does not specify azimuth and elevation angles, rendering the data challenging for humans to understand due to its complex structure. To address this, two prevalent signal processing methodologies

are employed to distinguish real objects with high intensity and obtain point clouds. The former is to first conduct a FFT along different TX-RX pairs to deduce the direction-of-arrival (DOA) of the target (step 5a), acquiring a 4D range-azimuth-elevation-Doppler tensor, while for 3D mmWave radars, the result is a 3D range-azimuth-Doppler tensor. Each cell within the 4D tensor corresponds to the intensity of the reflected signal. For DOA estimation, a MIMO antenna design is typically applied in mmWave FMCW radars. As illustrated in Fig. 5, the n TX antennas and m RX antennas form $n \times m$ virtual TX-RX pairs. To ensure signal separation, different TX antennas should transmit orthogonal signals. By analyzing the phase shift between different TX-RX pairs, distance differences between different pairs to the same target can be calculated. Furthermore, by considering the positional arrangement of the TX and RX antennas, the DOA of the target can be ascertained. At step 6a, the Constant False Alarm Rate (CFAR) algorithm [9] is typically implemented in the four dimensions to filter the tensor based on the intensity of each cell, thereby obtaining real targets in the format of point cloud for subsequent applications [10]. The CFAR algorithm sets dynamic intensity thresholds by comparing the intensity of each cell with its neighboring cells to realize a constant false alarm rate effect.

In contrast, the alternative signal processing workflow initially filters RD maps to generate target cells using also a CFAR-type algorithm (step 5b), then digital beamforming (DBF) is employed in step 6b to recover angular information and generate point clouds [8].

B. Methods to Lift from 3D to 4D

As previously discussed, the most crucial ability of 4D mmWave radars lies in their ability to measure the elevation dimension, which enriches the data from three-dimensional to four-dimensional space. The methodologies to achieve this enhancement can be categorized into hardware-based and software-based approaches, as detailed below:

1) *Hardware*: At the hardware level, there are two principal strategies to improve elevation resolution. The first is to increase the number of TX-RX pairs by simply cascading multiple standard mmWave radar chips [11] or integrating more antennas onto a single chip [12]. The second strategy aims to the effective aperture of the antennas by techniques such as meta-material [13].

2) *Software*: By virtually realizing hardware improvement or optimizing signal processing algorithms along the processing workflow, radar resolution can also be improved at the software level. Inspired by the synthetic aperture radar (SAR) technology, angular resolution can be increased by virtually expanding the aperture of antennas through software design [14]. Furthermore, innovative learning-based algorithms have the potential to replace traditional signal processing algorithms, such as FFT and CFAR [15] [16] thus facilitating a super-resolution effect.

C. Extrinsic Calibration

Given the relative sparsity and noise of radar point clouds, and the non-intuitive nature of spectrum data, it is a significant

challenge to calibrate radars with other sensors. While the enhanced resolution of 4D mmWave radars somewhat mitigates this issue, there remains a dearth of robust online calibration methods.

Following traditional calibration methods of 3D mmWave radars, corner reflectors are commonly employed to improve calibration accuracy. By carefully placing several corner reflectors and analyzing the sensing results of the 4D mmWave radar in conjunction with LiDAR and camera data, the extrinsic parameters can be calibrated [17]. In a departure from the conventional approach of calibrating each sensor pair sequentially, Domhof et al. calibrate all sensors simultaneously with respect to the body of mobile robot, achieving a median rotation error of a mere 0.02° [18]. By leveraging the Random Sample and Consensus (RANSAC) and Levenberg-Marquardt non-linear optimization, [19] accomplishes radar-camera calibration with only one single corner reflector, obviating the requirement of a specially designed calibration environment.

However, the practicability of corner reflectors in real-world scenarios is limited. Recent research has proposed calibration methods for 4D mmWave radars that eschew the need for specially placed corner reflectors, instead utilizing radar motion measurement to conduct online calibration for radars [20] or radar-camera pairs [21]. While these methods offer convenience, their efficacy under extreme weather conditions remains to be validated.

In light of the similar data structures of 4D mmWave radars and LiDARs, modifying conventional LiDAR-to-camera calibration methods [22] [23] is a promising avenue. Nevertheless, to address online joint calibration in extreme weather conditions, especially in the situation where LiDAR and camera have lousy performance, the potential of learning-based methods [24] warrants further exploration.

III. DATASETS

Public datasets play an indispensable role in the advancement of 4D mmWave radar-based algorithms, as they furnish essential platforms for the development, benchmarking, and comparative analysis of diverse algorithms, thereby stimulating research in the field. Current available datasets with 4D mmWave radars are introduced in this section, which are summarized in Table I.

We have curated published datasets according to the specific tasks they are tailored for, aiming to provide a comprehensive and systematically organized overview of datasets to aid the research and development of 4D mmWave radar-based algorithms.

A. Datasets for Perception

Datasets designed for 4D mmWave radar perception typically include 3D (or 2D) bounding boxes for object detection tasks, and tracking ID for object tracking tasks.

Public available 4D mmWave radar dataset are relatively rare. Astyx [25] represents the first dataset of its kind. The data consists of 500 synchronized frames (radar, LiDAR, camera) encompassing approximately 3,000 annotated 3D object annotations. As a pioneer dataset in the realm of 4D mmWave

TABLE I
4D MMWAVE RADAR DATASETS

Dataset	Resolution				Total Frames	Labeled Frames	Data Formats ¹	Modality ²	Bounding box	Tracking ID	Odometry
	Azi.	Ele.	Range(m)	Velo.(m/s)							
Astyx [25]	N/M ³	N/M	N/M	N/M	0.5K	0.5K	RPC	RCL	3D	✓	✗
SCORP [26]	15°	30°	12	0.33	3.9K	3.9K	ADC, RT, RPC	RC	✗	✗	✓
Coloradar [10]	1°	22.5°	0.12	0.25	108K	0K	ADC, RT, RPC	RLI	✗	✗	✓
Radatron [27]	1.2°	18°	0.05	N/M	152K	16K	ADC	RC	2D	✗	✗
RADIal [28]	0.1°	1°	0.2	0.1	25K	8.3K	ADC, RT, RPC	RCL	2D	✗	✓
RPDNet [29]	14.3°	57.2°	0.03	0.03	28K	0K	RT	RCLI	3D	✗	✓
VoD [30]	1.5°	1.5°	0.2	0.1	8.7K	8.7K	RPC	RCI	3D	✓	✓
TJ4DRadSet [17]	1°	1°	0.86	N/M	40K	7.8K	RPC	RCL	3D	✓	✓
K-Radar [31]	1°	1°	0.46	0.06	35K	35K	RT, RPC	RCLI	3D	✓	✓
MSC-RAD4R [3]	1°	0.5°	0.86	0.27	90K	0K	RPC	RCLI	✗	✗	✓
NTU4DRadarLM [32]	0.5°	0.1°	0.86	N/M	61K	0K	RPC	RCLIT	✗	✗	✓
Dual Radar [33]	1.2°	2°	0.22	N/M	50K	10K	RPC	RCL	3D	✓	✗

¹ADC: raw radar data after Analog-to-Digital Converter; RT: radar tensor representations like RA, RD, RAD or 4DRT; RPC: radar point cloud;

²R: Radar, C: Camera, L: LiDAR, I: IMU (Inertial Measurement Unit), T: Thermal Camera

³N/M: Not Mentioned.

radar, the volume of data in Astyx is relatively limited. The Radatron dataset [27] enhances the data resolution through a cascaded MIMO radar and provides radar heatmaps with 2D bounding boxes labeled by camera ground truth. However, as Radatron was collected under clear weather conditions, it is not much suitable for demonstrating radar performance under severe weather conditions.

In order to facilitate researchers in handling radar data in a more fundamental manner, the RADIal dataset [28] records sensor signals in their raw format. This raw signal corresponds to the ADC output. This ADC data serves as the foundation for generating various conventional radar representations, such as radar tensors and point clouds. Given that the raw ADC data is not interpretable by human eyes, the annotations in the RADIal dataset are presented as 2D bounding boxes in the image plane.

The VoD dataset [30] is a multi-sensor automotive dataset for multi-class 3D object detection, comprising calibrated and synchronized LiDAR, camera, and radar data. It contains 8693 frames of data captured in complex urban traffic scenarios, and includes 123106 3D bounding box annotations of both stationary and dynamic objects and tracking IDs for each annotated object. Road user detection is the primary concern of the VoD dataset, which therefore differentiates between pedestrian, cyclist, and car labels.

In a similar vein, the Tj4DRadSet dataset [17] comprises 44 consecutive sequences, totaling 7757 synchronized frames, well-labeled with 3D bounding boxes and trajectory IDs. Notably, the TJ4DRadSet dataset offers occlusion and truncation indicators in each object to distinguish between different levels of detection difficulty. This dataset encompasses eight categories: car, bus, truck, construction vehicle, pedestrian, motorcyclist, bicyclist, and tricyclist. Unlike the VoD dataset, Tj4DRadSet is characterized by its inclusion of a broader and more challenging array of driving scenario clips, such as urban roads, highways, and industrial parks.

To the best of our knowledge, K-Radar [31] currently contains most diverse scenarios in 4D mmWave radar datasets as it collects 35k frame under a variety of weather conditions, including sunny, foggy, rainy, and snowy. K-Radar not only

provides 4D mmWave radar data but also includes high-resolution LiDAR point clouds, surround RGB imagery from four stereo cameras, and RTK-GPS and IMU data from the ego-vehicle. Fig. 6 illustrates the comparison of different modality sensors across different weather conditions. It is worth mentioning that K-radar is currently the only dataset that provides 4D mmWave radar tensors. In order to facilitate experiments with various neural network architectures, K-radar also provides a visual programming tool to modularize the neural network training code.



Fig. 6. Data annotations in K-Radar dataset [31] across different weather conditions.

However, the 4D mmWave radar models employed in the aforementioned datasets are inconsistent, making it challenging for researchers to analyze and compare the performance of different 4D mmWave radar data. The recently unveiled Dual Radar dataset [33], as illustrated in Figure 7, encompasses two distinct types of mmWave radars, the Arbe Phoenix and the ARS548 RDI radar. The collection of 4D mmWave radar point clouds from these two radar types within identical scenes enables an investigation into the impact of different sparsity

levels in point clouds on object detection performance. This exploration is poised to lay the groundwork for furthering research on 4D mmWave radar technology in the autonomous vehicle sector.

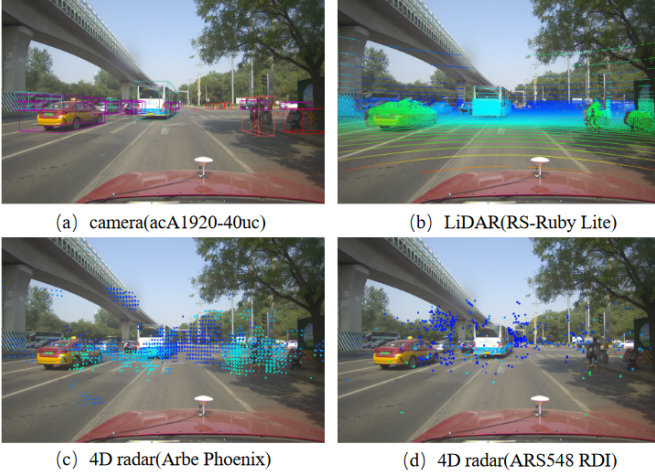


Fig. 7. The data visualization of Dual Radar dataset. [33]

B. Datasets for Localization and Mapping

4D mmWave radar is capable of generating dense 3D point clouds that incorporates elevation information, thereby facilitating robust localization even under challenging environmental conditions. In recent years, there has been a growing recognition of the critical significance of 4D mmWave radar in localization and mapping, leading to the public release of several 4D mmWave radar datasets specifically designed for these tasks. Odometry information is indispensable for localization, mapping, or Simultaneous Localization and Mapping (SLAM). Therefore, besides datasets specialized for localization and mapping, datasets introduced above can also be employed, provided they include odometry information. 4D mmWave radar technology is capable of generating a dense 3D point cloud that incorporates elevation information, thereby facilitating robust localization even under challenging environmental conditions. In recent years, the critical importance of 4D mmWave radar in localization and mapping has gained increasing recognition, leading to the public release of several 4D mmWave radar datasets specifically designed for these tasks. Odometry information is crucial for localization, mapping, or Simultaneous Localization and Mapping (SLAM). In addition to datasets specifically designed for these tasks, the datasets mentioned above can also be utilized for localization and mapping, provided they include odometry information.

ColoRadar [10] is a dataset dedicated to research on localization and mapping, comprising approximately 2 hours of data from radar, LiDAR, and the 6-DOF pose ground truth. It provides radar data of three processing levels: raw ADC data, 3D range-azimuth-elevation tensors derived by compressing the Doppler dimension of 4D mmWave radar tensors, and radar point clouds. This dataset collects data from a variety of unique indoor and outdoor environments, thus providing a diverse spectrum of sensor data. In the Colordar dataset, the radar

is mounted on a robot with a relatively restrained mobility profile without GNSS integration, thereby limiting access to ground truth information regarding the robot's position.

The MSC-RAD4R dataset [3] is a ROS-based 4D mmWave radar dataset for SLAM. It records data under a wide range of weather and environmental conditions, with the same route yielding data from both clear and snowy weather conditions for comparison. Additionally, MSC-RAD4R introduces artificially generated smoke environment data generated by a smoke machine, further emphasizing the robust capabilities of 4D mmWave radars.

The NTU4DRadLM dataset [32] is a recent contribution to this field. Distinguished from its predecessors, NTU4DRadLM delivers an extensive array of localization-relevant sensor data, including 4D mmWave radar, LiDAR, camera, IMU, GPS, and even a thermal camera. Curated explicitly for SLAM tasks, it provides fine-tuned ground truth odometry and supports closed-loop trajectory configurations to enable potential loop detection and back-end optimization. Accommodating varying sensor platform velocities, NTU4DRadLM's data is captured using both robotic and vehicular platforms. Furthermore, it encompasses a wide range of road conditions, encompassing structured, semi-structured, and unstructured roads, spanning both small-scale environments (e.g., gardens) and large-scale urban settings.

In addition, several datasets enumerated in Table I provide radar data with relatively low angular resolution [26], [29]. These datasets, which are not detailed within the scope of this paper, provide alternative radar data characteristics that may be leveraged in different research contexts.

C. Challenge

Taking into account the entirety of the datasets delineated afore, it becomes apparent that there is a lack of labeled radar ADC data required for deep radar detection. One possibility to overcome this deficiency is the employment of syntactic data generation methods that relies on some sensor model. Unfortunately, radar modeling is extremely challenging and computationally intensive due to the multiple effects that occur in acquisition, such as multi-path reflections, signal interference, reflective surface interactions, discrete resolution cells, and signal attenuation.

Moreover, current 4D mmWave radar datasets do not rival the voluminous scale of other autonomous driving datasets such as nuScenes [34] and ONCE [35]. The substantial size of datasets is imperative for the evaluation of algorithmic generalizability and for facilitating comparative analysis with other sensor modalities in the context of 4D mmWave radar research.

IV. LEARNING-BASED RADAR DATA ENHANCEMENT

Despite the extensive development of radar imaging technology over the years, traditional handcrafted methods such as CFAR continue to manifest inherent limitations. These methods, while foundational, often fail to account for the diverse and complex nature of real-world targets, which

can vary significantly in shape and extend across multiple-resolution cells. Such discrepancies can induce masking effects within CFAR-type algorithms, leading to a diminution in the resolution of point clouds and consequent information loss.

In response to the limitations of conventional methods, this section will pivot to exploring learning-based radar data quality improvement techniques. The advent of deep learning, particularly within the autonomous driving domain, offers promising avenues for addressing the deficiencies above. By leveraging the capabilities of deep learning, it is possible to develop more adaptive and robust algorithms that can improve the fidelity of radar imaging. Additionally, we will discuss the challenges we believe still exist in this area, thereby inspiring the research community.

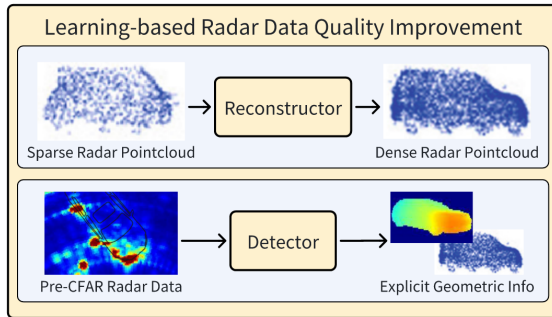


Fig. 8. Two dominant pipelines in learning-based radar data enhancement.

In the contemporary landscape of mmwave radar technology, two dominant pipelines have emerged based on learning methods. We categorize them as "Reconstructor" and "Detector". Their main difference are shown in Fig. 8.

A. Reconstructor

Reconstructor focuses on improving the resolution of previously acquired radar point clouds. This approach is dedicated to the post-processing enhancement of data fidelity, thereby increasing the detail and usefulness of the radar imagery.

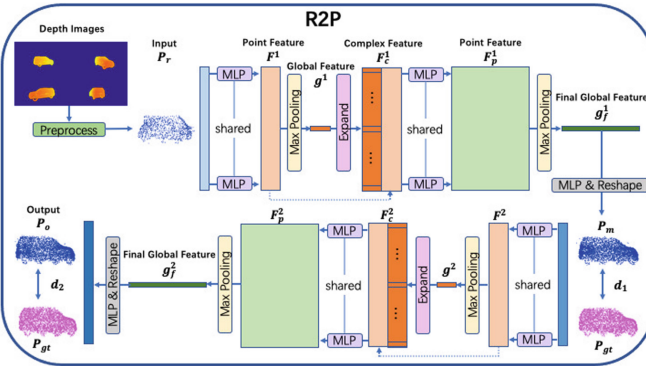


Fig. 9. R2P [36] network architecture

The related work is primarily inspired by the reconstruction of LiDAR point clouds, such as the PointNet [37] structure in [38], which in turn inspired the works of Sun et al. [39]

[36] [40]. Although these studies require data observed from different viewpoints of the target, which may constrain their immediate integration into autonomous driving systems, the underlying principles of their model architectures offer valuable insights. Specifically, the employment of a conditional Generative Adversarial Network (GAN) architecture facilitates the concurrent training of generator and discriminator networks, as detailed in [39]. Moreover, the innovative two-stage point cloud generation process, which incorporates a loss function that synergistically combines Chamfer Distance (CD) and Earth Mover's Distance (EMD) metrics, is elucidated in [36]. When confronted with coarse and sparse input point clouds, the methodologies proposed by Sun et al. have been validated to substantially surpass existing techniques, including PointNet [37], PointNet++ [41] and PCN [38]. The robustness of these methods underscores their potential to significantly enhance the accuracy and reliability of point cloud reconstruction, even in the presence of suboptimal input radar data.

B. Detector

Meanwhile, Detector signifies a substantial departure from traditional processing techniques. This innovative approach leverages neural networks to engage directly with raw radar data such as RD maps or 4D tensors, which circumvents conventional techniques such as CFAR or DBF, potentially leading to more efficient and robust detection capabilities in real-time applications.

Brodeski et al. [16] pioneer the application of Convolutional Neural Networks (CNNs) to RD maps for the detection and localization of multiple objects called DRD(deep radar detection) net. They reconceptualize the challenge of target detection within RD maps as a segmentation task and adopt a model structure analogous to the 2D-U-Net [42], renowned for its efficacy in medical image segmentation. Confronted with the scarcity of well-annotated RD map datasets, they devise a strategy to extract labeled radar data from the calibration process conducted within an anechoic chamber. Furthermore, they introduce a novel data augmentation method to enhance the diversity and volume of the dataset. Experiments of the DRD network demonstrate its capability to function in real-time, with inference times recorded at approximately 20ms. Notably, the DRD network has been shown to surpass classic methods in terms of detection accuracy and robustness. Though this work does not include real-world radar data with all the impairments that come along, the findings from this study unequivocally illustrate the considerable promise of neural network applications to radar complex data.

However, accurately labeling radar frequency data remains a formidable challenge. This is primarily due to disparities between data collected in the controlled environment of anechoic chambers and that obtained under real-world driving scenarios. The latter presents greater complexity with factors such as multi-path reflections, interference, attenuation, etc.

To address this challenge, Cheng et al. [8], [29] use LiDAR point clouds as the supervision and successively design network architectures inspired by U-Net [43] and Generative Adversarial Networks (GAN) [44]. In complex roadway

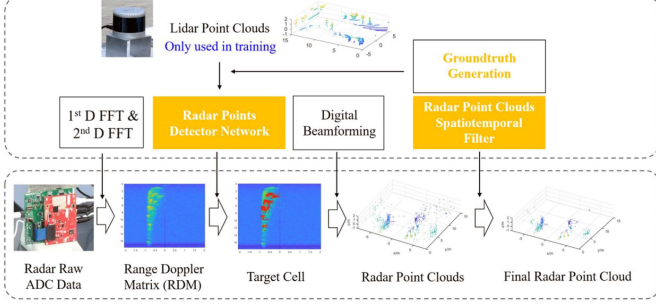


Fig. 10. Overview of the radar signal processing chain with [29]

scenes, the generated 4D mmWave radar point clouds by [29] not only demonstrate a reduction in clutter but also provide denser point clouds of real targets compared to the classical CFAR detectors. Additional comparisons on the performance of perception and localization tasks between the generated point cloud and traditional point cloud further prove the improvement of data quality.

C. Challenge

As noted in [27], [45], the diversity of mmWave radar hardware utilized across various datasets leads to significant variations in pre-CFAR data, making it challenging to construct a large-scale public dataset and benchmark. Furthermore, pre-CFAR data is far less intuitive than point cloud data, rendering the manual labeling process exceedingly laborious and difficult to achieve accuracy, hence producing high-quality supervised data for neural networks is problematic. Another avenue is the adoption of learning-based approaches for generating synthetic automotive radar scenes and data [46], [47]. However, as such methods are based on simulation, it depends on a world model that may contain inaccuracies. Additionally, the management of pre-CFAR data is associated with considerable computational and memory demands, necessitating a judicious balance between the requirements for computational power and the minimization of information loss.

V. PERCEPTION APPLICATIONS

Currently, the point cloud density of 4D mmWave radars has already attained a level comparable to that of low-beam LiDAR, with the added advantages of exhibiting superior robustness under low visibility and adverse weather conditions. Therefore, researchers have been attempting to transfer LiDAR point cloud processing models to 4D mmWave radars in various tasks, including target detection [51], [53], [54], trajectory tracking [55], [56], and scene flow prediction [57], [58], among others. Furthermore, as described in Section IV, pre-CFAR radar data encompasses a wealth of information, promoting some researchers to engage directly with RD maps or 4D tensors, bypassing point cloud generation tasks. Existing 4D mmWave radar point cloud and pre-CFAR data feature extraction methods in autonomous driving perception are summarized in Fig. 11, which will be detailed in this section.

In Section V-A, we review and analyze perception models for radar point clouds (RPC), which are primarily enhancements of LiDAR-based methodologies. The 4D mmWave radars branch of some fusion methods are also included. In Section V-B, we investigate the methods utilizing pre-CFAR radar data, including the range-frequency map, range-azimuth map, range-azimuth-Doppler cube, and 4D tensors. In Section V-C, the integration of 4D mmWave radars into multi-sensor fusion systems, as well as the effectiveness of such methods are present. In Section V-D, we discuss current challenges of this field.

A. Point Cloud Feature Extraction

Given the analogous nature of their data formats, it is clear that a significant number of RPC methodologies have their roots in LiDAR-based techniques. However, this transposition necessitates meticulous consideration of the inherent constraints associated with radar systems. These limitations encompass low-resolution representations, data sparsity, and inherent uncertainty within the data. Conversely, radar systems outperform in areas such as superior range resolution, velocity

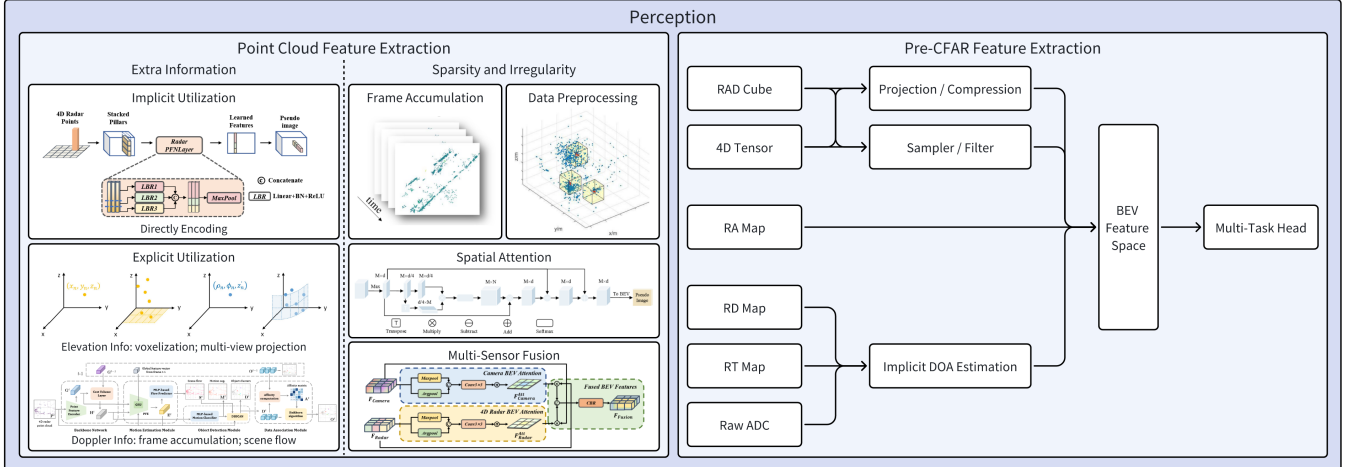


Fig. 11. Feature extraction methods for 4D mmWave radars in autonomous perception. Example images are from [48]–[52].

TABLE II
SUMMARY OF 4D-RADAR PERCEPTION METHODS

A. WITH RADAR POINTCLOUD

Task	Methods	Year	Modalities	Astyx 3D mAP(%)	VoD [30] mAP(%)	TJ4D mAP(%)
			Easy	Moderate	Entire	BEV
3D Object Detection	PointPillars [59] [‡]	2019	RPC	30.14	24.06	21.91
3D Object Detection	CenterPoint [60] [‡]	2021	RPC	-	-	45.42 [†]
3D Object Detection	PillarNeXt [61] [‡]	2023	RPC	-	-	42.23 [†]
3D Object Detection	RPEA-Net [52]	2021	RPC	38.85	32.19	30.57
3D Object Detection	MVFAN [49]	2023	RPC	45.60	39.52	38.53
3D Object Detection	RadarPillarNet [48]	2023	RPC	-	-	46.01 [†]
3D Object Detection	LXL-R [62]	2023	RPC	-	-	46.84 [†]
3D Object Detection	SMIFormer [63]	2023	RPC	-	-	48.77[†]
3D Object Detection	SMURF [51]	2023	RPC	-	-	50.97[†]
3D Object Detection	RadarMFNNet [50]	2023	RPC	-	-	69.72[†]
3D Object Detection	FUTR3D [64] [‡]	2023	C&RPC	-	-	49.03 [†]
3D Object Detection	BEVFusion [65] [‡]	2023	C&RPC	-	-	49.25 [†]
3D Object Detection	3DRC [66]	2019	C&RPC	61.00	48.00	45.00
3D Object Detection	Cui et al. [53]	2021	C&RPC	69.50	50.05	49.13
3D Object Detection	RCFusion [48]	2023	C&RPC	-	-	49.65
3D Object Detection	LXL [62]	2023	C&RPC	-	-	56.31
3D Object Detection	InterFusion [67]	2022	L&RPC	57.07	47.76	45.05
3D Object Detection	M^2 -Fusion [54]	2023	L&RPC	61.33	49.85	49.12

B. WITH PRE-CFAR DATA

Task	Methods	Year	Modalities	Radar Input	Seg. mIoU	RADlal [28](%)	RADlal [28](%)	K-Radar [31] mAP(%)
					Det. AP	Det. AR	3D Det. mAP	3D
Freespace Segmentation; 2D Object Detection	T-FFTRadNet [68]	2023	R	ADC	79.60	88.20	86.70	-
Freespace Segmentation; 2D Object Detection	T-FFTRadNet [68]	2023	R	RD	80.20	89.60	89.50	-
Freespace Segmentation; 2D Object Detection	ADCNet [69]	2023	R	ADC	78.59	95.00	89.00	-
Freespace Segmentation; 2D Object Detection	FFTDAshNet [70]	2023	R	RD	85.58	96.53	98.51	-
Freespace Segmentation; 2D Object Detection	FFTRadNet [28]	2022	R	RD	73.98	96.84	82.18	-
Freespace Segmentation; 2D Object Detection	TransRadar [71]	2024	R	RAD	81.10	97.30	98.40	-
Freespace Segmentation; 2D Object Detection	CMS [72]	2023	C&R	RD	80.40	96.90	83.49	-
Freespace Segmentation; 2D Object Detection	EchoFusion [73]	2023	C&R	RT	-	96.95	93.43	39.81
2D & 3D Object Detection	RTN [31]	2022	R	4DRT	-	-	-	68.35*
3D Object Detection	RTNH [31]	2022	R	4DRT	-	-	-	40.12
3D Object Detection	E-RTNH [74]	2023	R	4DRT	-	-	-	47.44
3D Object Detection	E-RTNH [74]	2023	R	4DRT	-	-	-	58.39
								59.40

Abbreviation about Modalities and Radar Input: R(Radar), C(Camera), L(Lidar), RPC(Radar Point Cloud), ADC(raw radar data after Analog-to-Digital Converter), RD(Range-Doppler map), RAD(Range-Azimuth-Doppler cube), RT(Range-Time map), 4DRT(Range-Azimuth-Elevation-Doppler Tensor)

[†] indicates data derived through multi-frame accumulation. Specifically, the methodologies referenced in relation to the VoD dataset employ detection points from 5 scans of radar data, whereas the RadarMFNNet [50] approach, as applied to the TJ4DRadSet, utilizes data from 4 consecutive frames.

[‡] denotes strategies originally conceptualized for LiDAR point clouds, which have been subsequently adapted and retrained utilizing radar datasets to serve as baseline comparisons. The comparative outcomes are directly inherited from [48], [49], [51], [52], [62].

* signifies data extracted from a subset comprising 20 sequences, which is part of the K-Radar dataset encompassing a total of 58 sequences.

measurement capabilities, and the advantage of early target detection. Consequently, these unique characteristics necessitate the development of specifically tailored network designs.

Upon a thorough review of the literature, it appears that Meyer et al. [66] pioneer the adaptation of a CNN architecture, originally designed for camera-LiDAR fusion [75], for the processing of 4D mmWave radar point clouds and RGB images. To reconcile the discrepancy in data formats, they elect to omit the Doppler information inherent to 4D mmWave radar data, instead solely utilize the spatial coordinates and intensity values. Subsequently, they employ the resulting point clouds to generate Bird's Eye View (BEV) images with six height maps and one density map to formulate three-dimensional (3D) object proposals. Remarkably, their fusion network demonstrates enhanced precision employing RPC instead of LiDAR point clouds, achieving an average precision (AP) of 61% on the Astyx dataset [25]. The authors postulate that this improvement may be attributable to the relatively sparse 16-beam configuration of the LiDAR sensor within the dataset. Although the authors recognise that this hypothesis need further exploration, the preliminary findings remain both intriguing and promising.

Regarding subsequent research, Table II offers a comprehensive and succinct exposition of the field. Building upon the foundation of existing work, these investigations have masterfully exploited the distinctive attributes of 4D mmWave radar point clouds, encompassing elements like elevation, Doppler data, and Radar Cross Section (RCS) intensity. Moreover, they have ingeniously formulated strategies to address the inherent sparsity and irregular distribution of these data points, thereby advancing the field significantly.

In light of the augmented elevation data presented by 4D mmWave radars, a distinct advancement over 3D mmWave radars, or the Doppler information, a feature not mirrored in LiDAR systems, most studies [30], [50], [52], [66], [67] have opted to reference the implicit structures like SECOND [76] and PointPillars [59]. These studies encode extra radar attributes directly, comparable to the conventional spatial coordinates x, y, z in point clouds. Palffy et al. [30] demonstrate that the addition of elevation data, Doppler information, and RCS information respectively increase the 3D mean Average Precision (mAP) with 6.1%, 8.9% and 1.4%. However, the result of the proposed method (47.0% mAP) is still far inferior to the LiDAR detector on 64-beam LiDAR (62.1% mAP), indicating that there is still room for improvement in the optimization of 4D mmWave radar-based detection methods. Nevertheless, Zheng et al. [48] introduce a subtle yet impactful modification, by proposing the Radar PillarNet backbone, colloquially termed RPNet. This structure employs three separate linear layers, each with unshared weights, to extract spatial position, velocity, and intensity features, respectively. Subsequently, a BEV pseudo image is generated. Ablation studies have demonstrated that RPNet enhances the 3D mAP by 4.26%.

Furthermore, to explicitly utilize the elevation information, Cui et al. [53], Yan et al. [49] and Shi et al. [63] have each explored extracting point cloud features from multiple viewpoints. In [53], radar point clouds are processed into Front

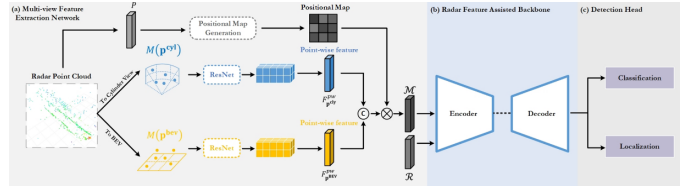


Fig. 12. The flowchart of multi-view feature extraction [49]

View (FV) and BEV perspectives. Features extracted from each view are subsequently fused with features derived from the camera branch. MVFAN [49] employs both BEV pillar and cylinder pillar methods to extract point cloud features. Conversely, SMIFormer [63] transforms point clouds into voxel features, which are then projected onto three distinct planes: FV, Side View (SV), and BEV. Following this, features are aggregated using intra-view self-attention and inter-view cross-attention mechanisms. Notably, this methodology is further refined by employing a sparse dimension compression technique, significantly reducing the memory and computational demands involved in converting 3D voxel features into 2D features.

Addressing the utilization of Doppler information, Tan et al. [50] delineate a widely-adopted yet efficacious technique. Recognizing that mmWave radars intrinsically measure the radial relative velocity of detected objects, and the motion of the vehicle itself results in different coordinate systems for multi-frame point clouds, they first calculate the vehicle's velocity, followed by compensating and obtaining each point's true velocity relative to the ground, which is often referred to as 'absolute velocity'. Moreover, the integration of Doppler information facilitates a more convenient and accurate accumulation of historical frame point clouds, thereby enhancing point cloud density. Yan et al. [49] further propose the Radar Feature Assisted Backbone. In this design, each point's absolute and relative velocities, along with its reflectivity, are integrated into position embeddings. These embeddings are then multiplied with the self-attention reweighting map of point-wise features, thereby enhancing the exchange of information at the feature vector level in a trainable fashion. On the other hand, Pan et al. [55] introduce a 'detection by tracking' strategy. This approach leverages velocity characteristics to achieve point-level motion segmentation and scene flow estimation. Subsequently, employing the classical DBSCAN clustering method suffices to surpass the tracking accuracy of established techniques like centerpoint [60] and AB3DMOT [77].

Another significant challenge in processing 4D mmWave radar point clouds is the inherent sparsity and irregular distribution. Considering the physical size constraints on the aperture of vehicular radars and the omnipresence of electromagnetic interference and multipath reflections in traffic environments, the resolution of 4D mmWave radar point clouds is considerably inferior to that of LiDAR, often resulting in a higher prevalence of clutter and noise. For instance, studies have noted that point clouds in the Astyx dataset struggle to articulate detailed features, which complicates the assessment of the orientation of detected objects [52]. Moreover, a considerable number of points are found to be distributed below

the ground plane [54], adversely affecting detection accuracy.

To mitigate these challenges, several improvement strategies have been proposed and employed. Common methods include the accumulation of multiple frame point clouds [50], [55], preprocessing and filtering of point clouds [51], [52], [54], employing spatial attention mechanisms to extract contextual information for feature enhancement [48], [49], [52], [63], and integrating information from different sensor modalities [48], [54], [62], [67].

To accumulate point clouds across multiple consecutive frames, as previously mentioned, the Doppler information plays a pivotal role. This can be achieved through ego-velocity estimation and motion compensation [50], or by motion segmentation and scene flow estimation [55], resulting in precision that surpasses mere simple stacking of point clouds.

Targeting at the preprocessing phase, InterFusion [67] and M2Fusion [54] utilize a Gaussian normal distribution to assess whether the vertical angle of point falls within a normal range, based on the Shapiro-Wilk (S-W) test [78]. This approach effectively filters out a substantial number of noise points that are below the ground plane in the Astyx dataset [25]. Additionally, SMURF [51] incorporates a point-wise kernel density estimation (KDE) branch, which calculates the density of point clouds within several predefined distance ranges, offering a detailed understanding of point distribution. The derived density information is then concatenated with pillarized features, resulting in enhanced BEV features. By refining the initial data, these methods lay a strong foundation for more accurate and reliable downstream processing.

In the domain of model backbone architecture, the incorporation of spatial attention mechanisms has been acknowledged as an effective strategy to address the sparsity and irregular distribution of point clouds. Xu et al. [52] implemented a self-attention mechanism to extract global information from the pillarized radar point cloud. Further advancing this concept, Shi et al. [63] augment different view features using a combination of self-attention and cross-attention mechanisms. While self-attention focuses on understanding the relationships within a single view, cross-attention extends this understanding across different views, thus enabling a more comprehensive and integrated feature representation. Yan et al. [49] take a different approach by utilizing the attention matrix inherent in the self-attention mechanism to differentiate and reweight foreground and background points and their respective features. They also introduce a binary classification auxiliary loss to aid the learning process. Additionally, several studies have used spatial attention to fuse multimodal sensor data, not only addressing the noise and sparsity in radar point clouds, but also leveraging the strengths of different sensor modalities. These methods will be further elaborated in Sect.V-C.

B. Pre-CFAR Feature Extraction

In the domain of millimeter-wave (mmWave) radar signal processing, techniques such as side lobe suppression and CFAR algorithms are integral for mitigating noise and minimizing false alarms. These methodologies facilitate the extraction of signal peaks, thereby reducing the volume of data and

decreasing computational demands. However, a consequential drawback of this approach is the sparsity of radar point clouds, characterized by diminished resolution. Given the profound advancements in the realm of deep learning, particularly in the processing of dense image data, a pivot in research focuses towards Pre-CFAR data is observed, aiming to utilize more underlying hidden information.

To our best knowledge, there are currently several datasets containing 4D mmWave radar Pre-CFAR data [26]–[28], [31], [79]. Notably, a subset of these datasets [26], [27], [79] is characterized by a relatively lower elevation resolution, exceeding 15 degrees. Consequently, our survey will predominantly focus on the methodologies employed within the high resolution datasets provided by [28], [31]. This section intends to elucidate the comprehensive pipeline and the enhancements tailored for optimizing the characteristics of 4D mmWave radar data.

As discussed in Section II-A, the 4D radar signal processing workflow employs FFT methodologies on raw ADC data to discretely process the four dimensions: range, Doppler, azimuth, and elevation. This processing culminates in the generation of diverse data representations, including the Range-Doppler (RD) map, Range-Azimuth (RA) map, Range-Azimuth-Doppler (RAD) cube, and ultimately, a 4D tensor. From 2D maps to 4D tensors, the complexity of extracted features varies. The more dimensions of information contained in the data, the higher the memory and computation costs will be for the feature extraction process. The extracted features are generally aligned to the RA axis in BEV under polar coordinates or the XY axis in Cartesian coordinates, connecting to detection or segmentation heads, serving as the foundational elements for subsequent detection or segmentation operations.

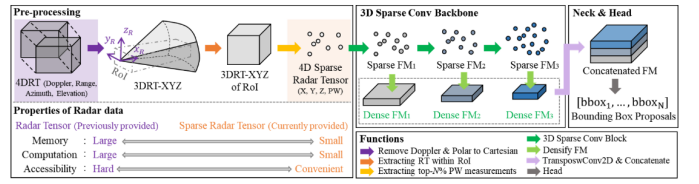


Fig. 13. Overview of RTNH [74] with 4D radar tensors

For the 4D radar tensor, Paek et al. [31], [74] opt to further extract a sparse tensor aligned to the Cartesian coordinate system, subsequently utilizing 3D sparse convolution to extract multi-scale spatial features. Experiments have demonstrated that retaining only the top-5% elements with the highest power measurements can maintain detection accuracy while significantly enhancing processing speed. Furthermore, the elevation information included in 4D tensors is essential facing 3D but not BEV 2D object detection.

In the context of RAD cube processing, TransRadar [71] projects the data onto the AD, RD, and RA planes, respectively, and innovatively designs an adaptive directional attention block to encode features separately.

Works related to the RD map [28], [68], [70] generally encode features along the RD dimensions using CNN or Swin Transformer structures. Subsequently, a noteworthy technique involves the transposition of the Doppler dimension with

the channel dimension, thereby redefining the conventional channel axis as the azimuth axis, followed by a series of deconvolution and upsampling steps to extrapolate features defined along the range-azimuth axes.

Conversely, RA map data, inherently aligned with the polar coordinate system, is amenable to direct processing through dense feature extraction networks. The generated BEV features are then either converted into the Cartesian coordinate system via bi-linear interpolation [27] or utilized within polar-based detection frameworks [73].

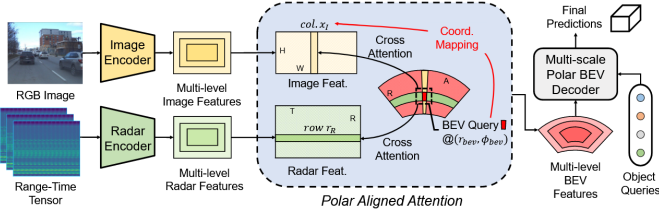


Fig. 14. Overview of Echofusion [73] with RT maps and images

Recently, some studies have also shifted towards addressing the elevated computational demands by performing FFT on raw ADC data. Consequently, strategies have emerged wherein raw ADC data is directly processed via complex-valued linear layers [68], utilizing the prior knowledge of the Fourier transform. Alternatively, Liu et al. [73] have leveraged data derived from a single-range FFT operation to generate Range-Time (RT) representations. Comparative analyses show the performance gap between the RT map and RA map with camera modality is within the error bar. These findings suggest that the resolution of azimuth angles and the permutation of Doppler-angle dimensions, as previously posited by Rebut et al. [28] and Giroux et al. [68], may not be requisite for achieving satisfactory performance outcomes.

C. Multi-Sensor Fusion Methods

Considering the capability of 4D mmWave radars to furnish point cloud data, several scholars have embarked on integrating this information with inputs from cameras or LiDAR systems to enhance the accuracy and robustness of the perception model. Generally, there are three fusion levels for different modalities: data level, feature level, and decision level. Existing research primarily focuses on the feature-level fusion.

As for 4DRV (4D mmWave Radar and Vision) fusion, 4D mmWave radars offer the ability to deliver high-precision depth and velocity information in a cost-effective manner, thereby mitigating the limitations inherent in camera systems and enhancing the accuracy of 3D detection. In recent studies, 4D mmWave radar signals are typically transformed into 2D image-like features, facilitating their practical deployment in conjunction with camera images. This fusion strategy leverages the strengths of both modalities, enabling a more comprehensive and accurate representation of the environment for advanced perception tasks.

Exemplifying this approach, Meyer et al. [66] employ a 3D region proposal network to camera images and BEV images

of the radar pointcloud, then meticulously crop, resize, and integrate multi-modal features for each proposed anchor. A subsequent study is performed by Cui et al. [53] with a novel self-supervised model adaptation block [80], which dynamically adapts the fusion of different modalities in accordance with the object properties. Besides, a FV map is generated from the 4D mmWave radar point clouds together with the BEV image. The presented method outperforms the former study [66] by up to 9.5% in 3D AP. The FV map effectively leverages the elevation information provided by 4D mmWave radars and achieves easier fusion with the monocular camera feature, balancing detection accuracy and computational efficiency.

Additionally, recent works such as RCFusion [48] and LXL [62] have advanced the integration of attention mechanisms for the fusion of image and 4D radar features. They begin by separately extracting BEV features from the camera and radar branches, then employ convolutional networks to create scale-consistent attention maps, effectively delineating the occupancy grid for target objects. The distinction lies in the fact that RCFusion [48] generates 2D attention maps in both the camera and radar branches, which are then multiplied with the BEV feature from the other modality. Conversely, LXL [62] solely utilizes the radar BEV feature to infer the 3D occupancy grid, which is then multiplied with the 3D image voxel features to achieve attention sampling of the image features.

Despite the notable advantages of 4DRV fusion, the vision-based branch may still struggle when facing aggressive lighting changes or adverse weather conditions, which in turn affects the overall performance of the model. Addressing this challenge, Wang et al. [67] first explore the advantages of 4DRL(4D mmWave Radar and LiDAR) fusion with an interaction-based fusion framework. They design an InterRAL (Interaction of Radar and LiDAR) module and update pillars from both modalities to enhance feature expression. The efficacy of this approach is substantiated through a series of ablation experiments, demonstrating the potential of this fusion strategy in improving the robustness and performance of perception models under challenging conditions.

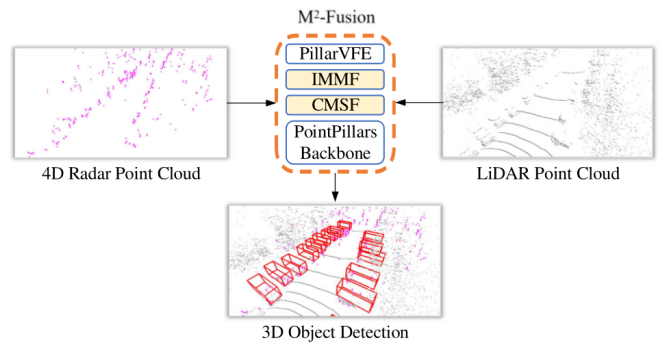


Fig. 15. Overview of the M^2 4DRL fusion model [54]

In a subsequent investigation, Wang et al. [54] propose the M^2 -Fusion network that integrates an interaction-based multi-modal fusion(IMMF) block and a center-based multi-

scale fusion(CMSF) block. Evaluated in the Astyx dataset [25], this novel approach outperforms mainstream LiDAR-based object detection methods significantly. As LiDARs can accurately detect objects at close range, 4D mmWave radars have a greater detection range owing to its penetrability, the fusion of 4DRL presents a promising technical solution that combines cost-effectiveness with high-quality performance.

D. Challenge

Current methodologies for 4D radar point cloud perception predominantly adapt established techniques from LiDAR applications, whereas approaches for pre-CFAR data often draw from the vision domain. Although the data formats exhibit similarities, the unique characteristics of mmWave radar data, specifically Doppler velocity and intensity information, warrant more focused attention for effective feature extraction. Moreover, pre-CFAR radar data characteristically contains a significantly higher ratio of background to actual objects (foreground) [71], a factor that complicates data interpretation and model training. The inherent noise within radar data further presents a substantial challenge for learning algorithms. The resilience of 4d radar models under out-of-distribution (OoD) conditions also remains inadequately explored and understood [31], which underscores the necessity for refined methodologies that can more accurately account for the distinct properties of mmWave radar data, thereby enhancing model robustness and performance in real-world scenarios.

VI. LOCALIZATION AND MAPPING APPLICATIONS

In challenging environments where satellite-based positioning is unreliable or high-definition maps are absent, localization and mapping by perception sensors becomes indispensable. A body of relevant research has been conducted utilizing the emerging 4D mmWave radars. Given that radar point clouds are significantly less data-intensive than their tensor counterparts, and methodologies developed for LiDARs can be adapted to 4D mmWave radar point clouds with minimal modifications, the majority of localization and mapping studies preferentially employ radar point clouds as their input data instead of radar tensors. As Fig16 demonstrates, the unique Doppler velocity information contained within radar point clouds presents a notable opportunity for exploitation, which will be discussed in Section VI-A. Subsequently, both traditional and learning-based localization and mapping approaches will be introduced in Section VI-B and Section VI-C, respectively. And Section VI-D briefly introduces current challenges in 4D mmWave radar-based localization and mapping.

A. Doppler Information Utilizing

The Doppler information constitutes a significant advantage of 4D mmWave radar, especially in the context of localization and mapping applications. Nevertheless, the optimal exploitation of this information within the autonomous driving sphere remains a relatively open question. Generally speaking, the utilization of Doppler information can be categorized into several categories:

1) Ego-Velocity Estimation: To estimate the ego-velocity of radar using Doppler information, a straightforward approach is the linear least squares (LSQ). Doppler velocity reflects the radial relative velocity between the object and the ego vehicle. Consequently, it is only the Doppler velocity from stationary objects that are viable for deducing the ego vehicle's velocity, while Doppler information from dynamic objects is considered as outliers. Under the assumption that the majority of surroundings points are from stationary objects, LSQ offers a suitable and computationally efficient method for ego-velocity estimation [89].

Assuming the 3D spatial coordinates of a point in the 4D mmWave radar system are denoted as \mathbf{p}_i . Its directional vector is determined as follows:

$$\mathbf{r}_i = \frac{\mathbf{p}_i}{\|\mathbf{p}_i\|}. \quad (3)$$

Let us consider a scenario where point \mathbf{p}_i is detected from a stationary object, the ideally measured Doppler velocity $v_{d,i}$ represents the projection of the ego-velocity \mathbf{v}_e onto the line-of-sight vector connecting the 4D mmWave radar with point \mathbf{p}_i . This velocity can be mathematically expressed as follows:

$$v_{d,i} = \mathbf{v}_e \cdot \mathbf{r}_i = v_{e,x} r_{i,x} + v_{e,y} r_{i,y} + v_{e,z} r_{i,z}. \quad (4)$$

For a set of N points constituting a single frame of the point cloud, the above equation can be generalized into a matrix formulation:

$$\begin{bmatrix} v_{d,1} \\ v_{d,2} \\ \dots \\ v_{d,N} \end{bmatrix} = \begin{bmatrix} r_{1,x} & r_{1,y} & r_{1,z} \\ r_{2,x} & r_{2,y} & r_{2,z} \\ \dots & \dots & \dots \\ r_{N,x} & r_{N,y} & r_{N,z} \end{bmatrix} \begin{bmatrix} v_{e,x} \\ v_{e,y} \\ v_{e,z} \end{bmatrix}. \quad (5)$$

Leveraging LSQ, an optimal solution can be obtained as follows:

$$\mathbf{v}_e = \begin{bmatrix} v_{e,x} \\ v_{e,y} \\ v_{e,z} \end{bmatrix} = (\mathbf{R}^T \mathbf{R})^{-1} \mathbf{R}^T \begin{bmatrix} v_{d,1} \\ v_{d,2} \\ \dots \\ v_{d,N} \end{bmatrix}, \quad (6)$$

where

$$\mathbf{R} = \begin{bmatrix} r_{1,x} & r_{1,y} & r_{1,z} \\ r_{2,x} & r_{2,y} & r_{2,z} \\ \dots & \dots & \dots \\ r_{N,x} & r_{N,y} & r_{N,z} \end{bmatrix}. \quad (7)$$

Indeed, relying solely on the LSQ method may result in substantial inaccuracies, primarily due to the influence of dynamic objects and noise. To mitigate these effects, specific research endeavors have implemented techniques such as RANSAC to effectively remove dynamic points before the application of LSQ [90].

An innovative enhancement to the conventional LSQ involves the incorporation of weighting mechanisms. Galeote-Luque et al. [91] weight each point by its signal power to diminish the influence of noise. Addressing the challenge posed by dynamic objects, Zhuang et al. [81] propose a

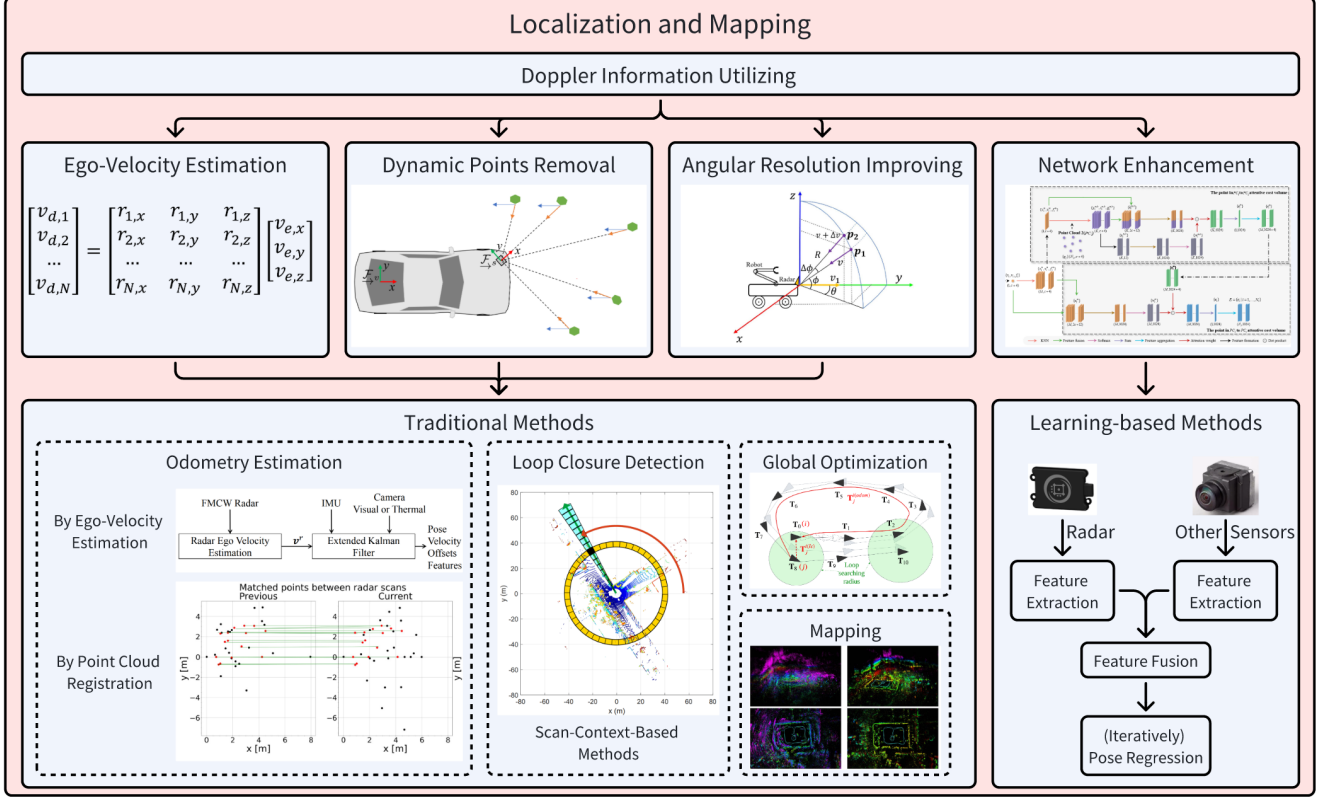


Fig. 16. The taxonomy of 4D mmWave radar-based localization and mapping. Example images are from [29], [81]–[88]

reweighted least squares method for the estimation of ego-velocity. The objective function is constructed as follows:

$$\min_{\mathbf{v}_e} \sum_{i=1}^n \lambda_i \|v_{d,i} - \mathbf{r}_i \cdot \mathbf{v}_e\|, \quad (8)$$

where λ_i denotes the weight of the i -th radar point. In the first iteration, $\lambda_i = 1$, and $\lambda_i = 1/(||v_{d,i} - \mathbf{r}_i \cdot \mathbf{v}_e|| + \epsilon)$, $\epsilon = 0.00001$. λ_i in the subsequent iterations, which quantifies the difference between the actual Doppler velocity $v_{d,i}$ and the ideal Doppler velocity assuming the i -th point originates from a stationary object, denoted as $\mathbf{r}_i \cdot \mathbf{v}_e$. Through iterative refinement, the weights of points from dynamic objects are progressively decreased, culminating in a more accurate computation of the ego-velocity \mathbf{v}_e . The RCS values are then employed to weight point cloud registration residuals to reduce the impact of matches with large RCS differences [92].

2) *Dynamic Points Removal*: Beyond ego-velocity estimation, another coherent exploration of Doppler information is to remove dynamic points, particularly leveraging the result derived from ego-velocity estimation. Zhang et al. [87] [93] apply a RANSAC-like method, while Zhuang et al. [81] utilize the weights to distinguish dynamic points in accordance with ego-velocity estimation.

3) *Angular Resolution Improving*: The angular resolution of 4D mmWave radars is determined by virtual TX-RX pairs mentioned in Section II, yet the range and Doppler resolution are dictated by the frequency disparity between transmitted

and received signals. Therefore, 4D mmWave radars typically exhibit superior performance in terms of range and Doppler resolution, as opposed to angular resolution. Cheng et al. [29] demonstrate that for two points from stationary objects, provided they share the same range and azimuth, the differences in elevation $\Delta\phi$ and Doppler Δv between the two points are interconnected. Similarly, the Doppler velocity resolution can also be converted into azimuth resolution. Hence, leveraging Doppler information can improve the angular resolution in particular azimuth and elevation ranges.

Drawing a parallel, Chen et al. [94] harness Doppler information to refine the point cloud and implement radar-inertial odometry using ground points, which exhibit stability in dynamic environments. Given that the resolution of the z coordinate in point clouds is generally inferior than Doppler resolution, once a point is identified as a ground point, its z coordinate can be recalculated using Doppler information and x, y coordinates. Adopting a strategy inspired by RANSAC, the authors hypothesize and refine ground points, then estimate ego-velocity iteratively. The refined point clouds can subsequently be applied in other tasks such as object detection.

4) *Network Enhancement*: In the context of learning-based localization and mapping, Doppler information also holds significant value. As previously discussed, Doppler velocity can serve as an indicator of whether a point originates from a stationary or dynamic object, which enlightens authors of [83] and [95] to establish a velocity-aware attention module.

This module leverages Doppler information to learn attention weights, thereby distinguishing between stationary and dynamic points.

B. Traditional Methods

Traditional localization and mapping refers to methods with no learning-based modules. Given the unique characteristic of 4D mmWave radars, related localization and mapping research mostly feature in odometry estimation and loop closure detection.

1) *Odometry Estimation*: Odometry estimation is the core of localization and serves as a crucial component of SLAM. A substantial body of traditional research on odometry estimation has been conducted in the context of 4D mmWave radars.

Considering the inherent noise and sparsity of 4D mmWave radar point clouds, initial odometry estimation research have primarily concentrates on the estimation of ego-velocity derived from the Doppler information instead of point cloud registration. Doer and Trommer make plenty of contributions to this field using Unmanned Aerial Vehicles (UAV). They fuse ego-velocity estimated by LSQ with the IMU data to perform UAV odometry estimation [89], [96], and further extend their work to multiple radars [97], [98] and radar-camera fusion systems [84]. As early investigations, these research efforts exhibit certain limitations. They rely on Manhattan world assumptions and consider the surroundings to be stationary, which may restrict the applicability in challenging outdoor scenarios.

The ego-velocity estimated by 4D mmWave radar point clouds has been employed by various researchers, in conjunction with additional assumptions, to achieve radar-based odometry. Ng et al. [82] present a continuous-time framework that fuse the ego-velocity from multiple radars with the measurement of an IMU. The continuity of this framework facilitates closed-form expressions for optimization and makes it well-suited for asynchronous sensor fusion. Given the relatively low elevation resolution of 4D mmWave radars in contrast to the more precise Doppler information, Chen et al. [94] propose a method to detect ground points and estimate ego velocity iteratively. Furthermore, Galeote-Luque et al. [91] combine the linear ego-velocity estimated from radar point clouds with the kinematic model of the vehicle to reconstruct the 3D motion of the vehicle. The authors assert that this method ensures short-term accuracy and rapid execution, qualifying it as an effective motion prior for more sophisticated SLAM frameworks.

Recent research has shifted focus from direct odometry estimation through ego-velocity, as seen in above studies, to point cloud registration akin to traditional LiDAR odometry. Michalczuk et al. [85] pioneer the realization of 3D point matching across sparse and noisy radar scans based on the classic Hungary algorithm [99]. Additionally, emerging research in 4D mmWave radar SLAM is also delving into point cloud registration techniques. Zhuang et al. [81] develop a 4D mmWave radar inertial odometry and mapping system named 4D iRIOM employing iterative Extended Kalman Filter (EKF). To mitigate the effects of sparsity, they introduce an innovative point cloud registration method between each

scan and submap. This method accounts for the local geometry of points in the current scan and the corresponding N nearest points in the submap, weighting the distances between them by their covariance to achieve a distribution-to-multi-distribution effect. The results of this approach are shown in Fig. 17. Moreover, they incorporate 4D iRIOM with GNSS and propose G-iRIOM [92], which further utilizes RCS value to weight the point cloud registration. Besides Zhang et al. [87], [93] apply the pose graph to construct a 4D mmWave radar SLAM system adapted from a well-known LiDAR SLAM method named hdl_graph_slam [100]. Building upon the traditional point cloud registration algorithm Generalized Iterative Closest Point (GICP) [101], they propose an adaptive probability distribution-GICP. This adaptation assigns different covariance to each point according to its uncertainty inferred from the coordinate of each point, acknowledging that points at greater distances may exhibit increased uncertainty. This design considers not only the geometric distribution of neighboring points but also the spatial variance of each point. Another 4D mmWave radar pose graph SLAM system named 4DRaSLAM is designed by Li et al [90]. This system incorporates the probability density function of each point to develop a probability-aware Normal Distributions Transform (NDT) [102] routine for scan-to-submap point cloud registration. Notably, the ego-velocity estimated from 4D mmWave radar Doppler information is utilized as a pre-integration factor in this system to replace the role of IMU.

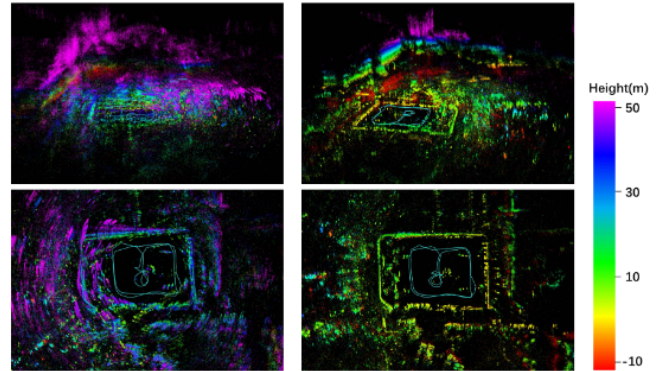


Fig. 17. The mapping performance of 4D iRIOM [81]

2) *Loop Closure Detection*: With respect to loop closure detection, relevant inventive research remains scarce. Existing 4D mmWave radar SLAM research that involve loop closure detection [81], [87], [90] typically reference the well-known Scan Context algorithm [86]. The original Scan Context algorithm partitions a LiDAR point cloud into several bins based on the azimuth, utilizing the maximum height of the points in each bin to encode the entire point cloud into an image. However, considering the relatively low resolution of height information provided by 4D mmWave radars, maximum intensity instead of height is adapted as context for loop closure detection in these systems.

C. Learning-based Methods

Research on learning-based 4D mmWave radar localization and mapping has predominantly focused on odometry estimation, replacing traditional point cloud registration and pose regression by deep networks.

As the originator, Lu et al. [88] extract the features from radar point clouds and IMU data by CNNs and Recurrent Neural Networks (RNNs), respectively. Subsequently, they innovatively propose a two-stage cross-modal attention mechanism to integrate these features effectively. Additionally, an RNN is utilized to capture the long-term temporal dynamics of the system. The efficacy of their approach is further enhanced when supplemented with data from RGB or depth cameras.

Recently, 4DRO-Net [83] establishes a coarse-to-fine hierarchical optimization framework that leverages a sliding window approach to iteratively estimate and refine pose estimation. With the help of a velocity-aware attention cost volume network, a feature extraction network is constructed to extract global-level and point-level features. These features are instrumental in generating initial pose estimations and subsequent corrections. The integration of these two pose constructs facilitates the derivation of an enhanced odometry estimation. Based on 4DRO-Net, Zhuo et al. present 4DRVO-Net [95], further extracts and fuses image features with 4D mmWave radar point cloud features. Fig. 18 displays the pipeline. The adaptive fusion module employs a deformable attention-based spatial cross-attention mechanism to align each 4D mmWave radar feature with corresponding image feature to achieve optimal fusion.

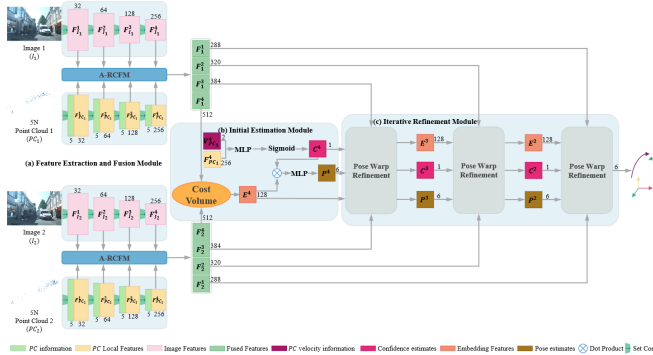


Fig. 18. The fusion and localization pipeline of 4DRVO-Net [95]

All these advanced learning-based radar odometry methods perform odometry estimation in an end-to-end fashion, i.e., the network ingests 4D mmWave radar point clouds (supplemented with images for fusion methods), and directly outputs odometry estimation. This benefits research on comprehensive end-to-end autonomous driving systems.

D. Challenge

The Doppler velocity inherent in 4D mmWave radar point clouds has been recognized and utilized in localization and mapping to realize ego-velocity estimation and dynamic object removal, etc. However, considering adequate semantic information provided by 4D mmWave radars, such as intensity,

traditional 3D registration methods like ICP may be less effective. Therefore, the exploration of learning-based methods or feature-based registration could yield more effective results. Regarding mapping, the sparsity of 4D mmWave radar point clouds presents a significant challenge. A potential solution could lie in mapping the environment using 4D tensor-level data, which may enhance the mapping performance.

VII. FUTURE TRENDS

4D mmWave radars have the potential to bring about transformative advancements in the field of autonomous vehicles. Nonetheless, it is far from mature at the moment. The prospective evolution of 4D mmWave radar technology in autonomous driving is likely to be contingent upon advancements in several key domains.

1) *Point Cloud Enhancement:* As the most commonly applied data format, 4D mmWave radar point clouds undergo evident inferior quality compared with other sensors — the characteristics of radars, such as the multi-path effect, severely degrade the fidelity of point clouds. Consequently, there is an urgent need to mitigate information loss throughout the signal processing workflow, particularly by replacing CFAR with precisely engineered learning-based algorithms. Additionally, the exploration of learning-based methods DOA estimation could supplant DBF techniques, potentially leading to super-resolution in angular estimation.

2) *Application Algorithms Redesign:* Beyond the quality enhancement of 4D mmWave radar point clouds, the post-signal processing application algorithms also warrant significant attention. Up till now, numerous application algorithms for 4D mmWave radars have been modified from their LiDAR counterparts. The unique attributes of 4D mmWave radars, such as their velocity measuring ability and adaptability in extreme environments, should be further explored by future research. For perception tasks, the fusion of multiple modalities is unquestionably a pivotal direction for future development. However, it remains to be determined whether the integration of additional sensor modalities might weaken the robustness of 4D mmWave radars in extreme weather conditions. As for 4D mmWave radar localization and mapping, the Doppler information utilizing, and sensor fusion with LiDARs and cameras offer vast expanses of potential, ripe for discovery and innovation.

3) *Pre-CFAR Data Utilization:* Regarding the distinctive data formats throughout the 4D mmWave radar signal processing workflow, such as raw ADC data, RD maps, and 4D tensors, their utilization for perception, localization and mapping tasks represents an interesting yet largely unexplored area of research. The development of learning-based models that can effectively leverage the information contained within these data formats, while maintaining satisfactory real-time performance, could potentially emerge as a focal point in future research endeavors.

4) *Dataset Enriching:* As with all other data-driven research domains, datasets pertaining to 4D mmWave radars play a significant role in facilitating related studies. However, existing datasets that incorporate 4D mmWave radars are relatively rare. The expansion of data formats and the enrichment

of scenario diversity are two critical fields waiting for further development.

VIII. CONCLUSION

This paper offers a comprehensive overview of the role and potential of 4D mmWave radars in autonomous driving. It sequentially delves into the signal processing theory, datasets, learning-based data quality improvement methods, application algorithms in perception, localization and mapping. Furthermore, it casts a forward-looking gaze towards future trends and potential avenues for innovation in this rapidly evolving field. The exploration of 4D mmWave radars within the realm of autonomous driving is an ongoing endeavor. This comprehensive review serves as both a primer for those new to the field and a resource for seasoned researchers, offering insights into the current state of the art and highlighting the potential for future developments.

REFERENCES

- [1] M. Jiang, G. Xu, H. Pei, Z. Feng, S. Ma, H. Zhang, and W. Hong, “4D High-Resolution Imagery of Point Clouds for Automotive mmWave Radar,” *IEEE Transactions on Intelligent Transportation Systems*, pp. 1–15, 2023.
- [2] “High Resolution Virtual AI Software for Imaging Radar - Oculii,” <https://www.oculi.com/>.
- [3] M. Choi, S. Yang, S. Han, Y. Lee, M. Lee, K. H. Choi, and K.-S. Kim, “MSC-RAD4R: ROS-Based Automotive Dataset With 4D Radar,” *IEEE Robotics and Automation Letters*, pp. 1–8, 2023.
- [4] I. Bilik, O. Longman, S. Villeval, and J. Tabrikian, “The Rise of Radar for Autonomous Vehicles: Signal Processing Solutions and Future Research Directions,” *IEEE Signal Processing Magazine*, vol. 36, no. 5, pp. 20–31, Sep. 2019.
- [5] A. Venon, Y. Dupuis, P. Vasseur, and P. Merriaux, “Millimeter Wave FMCW RADARS for Perception, Recognition and Localization in Automotive Applications: A Survey,” *IEEE Transactions on Intelligent Vehicles*, vol. 7, no. 3, pp. 533–555, Sep. 2022.
- [6] K. Harlow, H. Jang, T. D. Barfoot, A. Kim, and C. Heckman, “A New Wave in Robotics: Survey on Recent mmWave Radar Applications in Robotics,” May 2023.
- [7] S. Abdulatif, Q. Wei, F. Aziz, B. Kleiner, and U. Schneider, “Micro-doppler based human-robot classification using ensemble and deep learning approaches,” in *2018 IEEE Radar Conference (RadarConf18)*, Apr. 2018, pp. 1043–1048.
- [8] Y. Cheng, J. Su, H. Chen, and Y. Liu, “A New Automotive Radar 4D Point Clouds Detector by Using Deep Learning,” in *ICASSP 2021 - 2021 IEEE International Conference on Acoustics, Speech and Signal Processing (ICASSP)*, Jun. 2021, pp. 8398–8402.
- [9] H. Rohling, “Radar CFAR Thresholding in Clutter and Multiple Target Situations,” *IEEE Transactions on Aerospace and Electronic Systems*, vol. AES-19, no. 4, pp. 608–621, Jul. 1983.
- [10] A. Kramer, K. Harlow, C. Williams, and C. Heckman, “ColoRadar: The direct 3D millimeter wave radar dataset,” *The International Journal of Robotics Research*, vol. 41, no. 4, pp. 351–360, Apr. 2022.
- [11] A. Och, C. Pfeffer, J. Schrattecker, S. Schuster, and R. Weigel, “A Scalable 77 GHz Massive MIMO FMCW Radar by Cascading Fully-Integrated Transceivers,” in *2018 Asia-Pacific Microwave Conference (APMC)*, Nov. 2018, pp. 1235–1237.
- [12] R. Q. Charles, H. Su, M. Kaichun, L. J. Guibas, P. Ritter, M. Geyer, T. Gloekler, X. Gai, T. Schwarzenberger, G. Treter, Y. Yu, and G. Vogel, “A Fully Integrated 78 GHz Automotive Radar System-on-Chip in 22nm FD-SOI CMOS,” in *2020 17th European Radar Conference (EuRAD)*, Jan. 2021, pp. 57–60.
- [13] J. Jiang, Y. Li, L. Zhao, and X. Liu, “Wideband MIMO Directional Antenna Array with a Simple Meta-material Decoupling Structure for X-Band Applications,” *The Applied Computational Electromagnetics Society Journal (ACES)*, pp. 556–566, May 2020.
- [14] Z. Wu, L. Zhang, and H. Liu, “Generalized Three-Dimensional Imaging Algorithms for Synthetic Aperture Radar With Metamaterial Apertures-Based Antenna,” *IEEE Access*, vol. 7, pp. 59 716–59 727, 2019.
- [15] H.-W. Cho, W. Kim, S. Choi, M. Eo, S. Khang, and J. Kim, “Guided Generative Adversarial Network for Super Resolution of Imaging Radar,” in *2020 17th European Radar Conference (EuRAD)*. New York: Ieee, Jan. 2021, pp. 144–147.
- [16] D. Brodeski, I. Bilik, and R. Giryes, “Deep Radar Detector,” in *2019 IEEE Radar Conference (RadarConf)*, Apr. 2019, pp. 1–6.
- [17] L. Zheng, Z. Ma, X. Zhu, B. Tan, S. Li, K. Long, W. Sun, S. Chen, L. Zhang, M. Wan, L. Huang, and J. Bai, “TJ4DRadSet: A 4D Radar Dataset for Autonomous Driving,” in *2022 IEEE 25th International Conference on Intelligent Transportation Systems (ITSC)*, Oct. 2022, pp. 493–498.
- [18] J. Domhof, J. F. P. Kooij, and D. M. Gavrila, “A Joint Extrinsic Calibration Tool for Radar, Camera and Lidar,” *IEEE Transactions on Intelligent Vehicles*, vol. 6, no. 3, pp. 571–582, Sep. 2021.
- [19] L. Cheng, A. Sengupta, and S. Cao, “3D Radar and Camera Co-Calibration: A flexible and Accurate Method for Target-based Extrinsic Calibration,” in *2023 IEEE Radar Conference (RadarConf23)*, May 2023, pp. 1–6.
- [20] Y. Bao, T. Mahler, A. Pieper, A. Schreiber, and M. Schulze, “Motion Based Online Calibration for 4D Imaging Radar in Autonomous Driving Applications,” in *2020 German Microwave Conference (GeMiC)*, Mar. 2020, pp. 108–111.
- [21] E. Wise, J. Persic, C. Grebe, I. Petrovic, and J. Kelly, “A Continuous-Time Approach for 3D Radar-to-Camera Extrinsic Calibration,” in *2021 IEEE International Conference on Robotics and Automation (ICRA)*, May 2021, pp. 13 164–13 170.
- [22] A. Dhall, K. Chelani, V. Radhakrishnan, and K. M. Krishna, “LiDAR-camera calibration using 3D-3D point correspondences,” *arXiv preprint arXiv:1705.09785*, 2017.
- [23] Z. Pusztai and L. Hajder, “Accurate calibration of LiDAR-camera systems using ordinary boxes,” in *Proceedings of the IEEE International Conference on Computer Vision Workshops*, 2017, pp. 394–402.
- [24] C. Schöller, M. Schnettler, A. Krämer, G. Hinz, M. Bakovic, M. Güzet, and A. Knoll, “Targetless Rotational Auto-Calibration of Radar and Camera for Intelligent Transportation Systems,” Jul. 2019.
- [25] M. Meyer and G. Kuschk, “Automotive Radar Dataset for Deep Learning Based 3D Object Detection,” in *2019 16th European Radar Conference (EuRAD)*, Oct. 2019, pp. 129–132.
- [26] F. E. Nowruzi, D. Kolhatkar, P. Kapoor, F. Al Hassanat, E. J. Heravi, R. Laganiere, J. Rebut, and W. Malik, “Deep Open Space Segmentation using Automotive Radar,” in *2020 IEEE MTT-S International Conference on Microwaves for Intelligent Mobility (ICMIM)*, Nov. 2020, pp. 1–4.
- [27] S. Madani, J. Guan, W. Ahmed, S. Gupta, and H. Hassanieh, “Radatron: Accurate Detection Using Multi-resolution Cascaded MIMO Radar,” in *Lecture Notes in Computer Science*, ser. Lecture Notes in Computer Science, S. Avidan, G. Brostow, M. Cissé, G. M. Farinella, and T. Hassner, Eds. Cham: Springer Nature Switzerland, 2022, pp. 160–178.
- [28] J. Rebut, A. Ouaknine, W. Malik, and P. Perez, “Raw High-Definition Radar for Multi-Task Learning,” in *2022 IEEE/CVF Conference on Computer Vision and Pattern Recognition (CVPR)*, Jun. 2022, pp. 17 000–17 009.
- [29] Y. Cheng, J. Su, M. Jiang, and Y. Liu, “A Novel Radar Point Cloud Generation Method for Robot Environment Perception,” *IEEE Transactions on Robotics*, vol. 38, no. 6, pp. 3754–3773, Dec. 2022.
- [30] A. Palfy, E. Pool, S. Baratam, J. F. P. Kooij, and D. M. Gavrila, “Multi-Class Road User Detection With 3+1D Radar in the View-of-Delft Dataset,” *IEEE Robotics and Automation Letters*, vol. 7, no. 2, pp. 4961–4968, Apr. 2022.
- [31] D.-H. Paek, S.-H. Kong, and K. T. Wijaya, “K-Radar: 4D Radar Object Detection for Autonomous Driving in Various Weather Conditions,” in *Thirty-Sixth Conference on Neural Information Processing Systems Datasets and Benchmarks Track*, 2022.
- [32] J. Zhang, H. Zhuge, Y. Liu, G. Peng, Z. Wu, H. Zhang, Q. Lyu, H. Li, C. Zhao, D. Kircali, S. Mharolkar, X. Yang, S. Yi, Y. Wang, and D. Wang, “NTU4DRadLM: 4D Radar-centric Multi-Modal Dataset for Localization and Mapping,” Sep. 2023.
- [33] X. Zhang, L. Wang, J. Chen, C. Fang, L. Yang, Z. Song, G. Yang, Y. Wang, X. Zhang, J. Li, Z. Li, Q. Yang, Z. Zhang, and S. S. Ge, “Dual Radar: A Multi-modal Dataset with Dual 4D Radar for Autonomous Driving,” Nov. 2023.
- [34] H. Caesar, V. Bankiti, A. H. Lang, S. Vora, V. E. Lioung, Q. Xu, A. Krishnan, Y. Pan, G. Baldan, and O. Beijbom, “nuScenes: A Multimodal Dataset for Autonomous Driving,” in *2020 IEEE/CVF Conference on Computer Vision and Pattern Recognition (CVPR)*. Seattle, WA, USA: IEEE, Jun. 2020, pp. 11 618–11 628.

- [35] J. Mao, M. Niu, C. Jiang, H. Liang, J. Chen, X. Liang, Y. Li, C. Ye, W. Zhang, Z. Li, J. Yu, H. Xu, and C. Xu, “One Million Scenes for Autonomous Driving: ONCE Dataset,” Oct. 2021.
- [36] Y. Sun, H. Zhang, Z. Huang, and B. Liu, “R2P: A Deep Learning Model from mmWave Radar to Point Cloud,” in *Lecture Notes in Computer Science*, ser. Lecture Notes in Computer Science, E. Pimenidis, P. Angelov, C. Jayne, A. Papaleonidas, and M. Aydin, Eds. Cham: Springer International Publishing, 2022, pp. 329–341.
- [37] R. Q. Charles, H. Su, M. Kaichun, L. J. Guibas, P. Ritter, M. Geyer, T. Gloekler, X. Gai, T. Schwarzenberger, G. Tretter, Y. Yu, and G. Vogel, “PointNet: Deep Learning on Point Sets for 3D Classification and Segmentation,” in *2020 17th European Radar Conference (EuRAD)*. Honolulu, HI: IEEE, Jan. 2021, pp. 77–85.
- [38] W. Yuan, T. Khot, D. Held, C. Mertz, and M. Hebert, “PCN: Point Completion Network,” in *2018 International Conference on 3D Vision (3DV)*, Sep. 2018, pp. 728–737.
- [39] Y. Sun, Z. Huang, H. Zhang, Z. Cao, and D. Xu, “3DRIMR: 3D Reconstruction and Imaging via mmWave Radar based on Deep Learning,” in *2021 IEEE International Performance, Computing, and Communications Conference (IPCCC)*, Oct. 2021, pp. 1–8.
- [40] Y. Sun, Z. Huang, H. Zhang, and X. Liang, “3D Reconstruction of Multiple Objects by mmWave Radar on UAV,” in *2022 IEEE 19th International Conference on Mobile Ad Hoc and Smart Systems (MASS)*, Oct. 2022, pp. 491–495.
- [41] C. R. Qi, L. Yi, H. Su, and L. J. Guibas, “PointNet++: Deep Hierarchical Feature Learning on Point Sets in a Metric Space,” in *Advances in Neural Information Processing Systems*, vol. 30. Curran Associates, Inc., 2017.
- [42] C. Zhang, W. Luo, and R. Urtasun, “Efficient Convolutions for Real-Time Semantic Segmentation of 3D Point Clouds,” in *2018 International Conference on 3D Vision (3DV)*, Sep. 2018, pp. 399–408.
- [43] O. Ronneberger, P. Fischer, and T. Brox, “U-Net: Convolutional Networks for Biomedical Image Segmentation,” in *Lecture Notes in Computer Science*, ser. Lecture Notes in Computer Science, N. Navab, J. Hornegger, W. M. Wells, and A. F. Frangi, Eds. Cham: Springer International Publishing, 2015, pp. 234–241.
- [44] P. Luc, C. Couprise, S. Chintala, and J. Verbeek, “Semantic Segmentation using Adversarial Networks,” in *NIPS Workshop on Adversarial Training*, 2016.
- [45] I. Orr, M. Cohen, and Z. Zalevsky, “High-resolution radar road segmentation using weakly supervised learning,” *Nature Machine Intelligence*, vol. 3, no. 3, pp. 239–246, Mar. 2021.
- [46] U. Chipengo, “High Fidelity Physics-Based Simulation of a 512-Channel 4D-Radar Sensor for Automotive Applications,” *IEEE Access*, vol. 11, pp. 15 242–15 251, 2023.
- [47] B. Tan, L. Zheng, Z. Ma, J. Bai, X. Zhu, and L. Huang, “Learning-based 4D Millimeter Wave Automotive Radar Sensor Model Simulation for Autonomous Driving Scenarios,” in *2023 7th International Conference on Machine Vision and Information Technology (CMVIT)*, Mar. 2023, pp. 123–128.
- [48] L. Zheng, S. Li, B. Tan, L. Yang, S. Chen, L. Huang, J. Bai, X. Zhu, and Z. Ma, “RCFusion: Fusing 4-D Radar and Camera With Bird’s-Eye View Features for 3-D Object Detection,” *IEEE Transactions on Instrumentation and Measurement*, vol. 72, pp. 1–14, 2023.
- [49] Q. Yan and Y. Wang, “MVFAN: Multi-View Feature Assisted Network for 4D Radar Object Detection,” Oct. 2023.
- [50] B. Tan, Z. Ma, X. Zhu, S. Li, L. Zheng, S. Chen, L. Huang, and J. Bai, “3D Object Detection for Multiframe 4D Automotive Millimeter-Wave Radar Point Cloud,” *IEEE Sensors Journal*, vol. 23, no. 11, pp. 11 125–11 138, Jun. 2023.
- [51] J. Liu, Q. Zhao, W. Xiong, T. Huang, Q.-L. Han, and B. Zhu, “SMURF: Spatial Multi-Representation Fusion for 3D Object Detection with 4D Imaging Radar,” *IEEE Transactions on Intelligent Vehicles*, pp. 1–14, 2023.
- [52] B. Xu, X. Zhang, L. Wang, X. Hu, Z. Li, S. Pan, J. Li, and Y. Deng, “RPFANet: A 4D RaDAR Pillar Feature Attention Network for 3D Object Detection,” in *2021 IEEE International Intelligent Transportation Systems Conference (ITSC)*, Sep. 2021, pp. 3061–3066.
- [53] H. Cui, J. Wu, J. Zhang, G. Chowdhary, and W. R. Norris, “3D Detection and Tracking for On-road Vehicles with a Monovision Camera and Dual Low-cost 4D mmWave Radars,” in *2021 IEEE International Intelligent Transportation Systems Conference (ITSC)*, Sep. 2021, pp. 2931–2937.
- [54] L. Wang, X. Zhang, J. Li, B. Xv, R. Fu, H. Chen, L. Yang, D. Jin, and L. Zhao, “Multi-Modal and Multi-Scale Fusion 3D Object Detection of 4D Radar and LiDAR for Autonomous Driving,” *IEEE Transactions on Vehicular Technology*, vol. 72, no. 5, pp. 5628–5641, May 2023.
- [55] Z. Pan, F. Ding, H. Zhong, and C. X. Lu, “Moving Object Detection and Tracking with 4D Radar Point Cloud,” Sep. 2023.
- [56] B. Tan, Z. Ma, X. Zhu, S. Li, L. Zheng, L. Huang, and J. Bai, “Tracking of Multiple Static and Dynamic Targets for 4D Automotive Millimeter-Wave Radar Point Cloud in Urban Environments,” *Remote Sensing*, vol. 15, no. 11, p. 2923, Jan. 2023.
- [57] F. Ding, Z. Pan, Y. Deng, J. Deng, and C. X. Lu, “Self-Supervised Scene Flow Estimation With 4-D Automotive Radar,” *IEEE Robotics and Automation Letters*, vol. 7, no. 3, pp. 8233–8240, Jul. 2022.
- [58] F. Ding, A. Palffy, D. M. Gavrila, and C. X. Lu, “Hidden Gems: 4D Radar Scene Flow Learning Using Cross-Modal Supervision,” in *Proceedings of the IEEE/CVF Conference on Computer Vision and Pattern Recognition*, 2023, pp. 9340–9349.
- [59] A. H. Lang, S. Vora, H. Caesar, L. Zhou, J. Yang, and O. Beijbom, “PointPillars: Fast Encoders for Object Detection From Point Clouds,” in *2019 IEEE/CVF Conference on Computer Vision and Pattern Recognition (CVPR)*, Jun. 2019, pp. 12 689–12 697.
- [60] T. Yin, X. Zhou, and P. Krahenbuhl, “Center-based 3D Object Detection and Tracking,” in *2021 IEEE/CVF Conference on Computer Vision and Pattern Recognition (CVPR)*, Jun. 2021, pp. 11 779–11 788.
- [61] J. Li, C. Luo, and X. Yang, “PillarNeXt: Rethinking Network Designs for 3D Object Detection in LiDAR Point Clouds,” in *2023 IEEE/CVF Conference on Computer Vision and Pattern Recognition (CVPR)*, Jun. 2023, pp. 17 567–17 576.
- [62] W. Xiong, J. Liu, T. Huang, Q.-L. Han, Y. Xia, and B. Zhu, “LXL: LiDAR Excluded Lean 3D Object Detection with 4D Imaging Radar and Camera Fusion,” Aug. 2023.
- [63] W. Shi, Z. Zhu, K. Zhang, H. Chen, Z. Yu, and Y. Zhu, “SMIFormer: Learning Spatial Feature Representation for 3D Object Detection from 4D Imaging Radar via Multi-View Interactive Transformers,” *Sensors*, vol. 23, no. 23, p. 9429, Jan. 2023.
- [64] X. Chen, T. Zhang, Y. Wang, Y. Wang, and H. Zhao, “FUTR3D: A Unified Sensor Fusion Framework for 3D Detection,” Apr. 2023.
- [65] Z. Liu, H. Tang, A. Amini, X. Yang, H. Mao, D. L. Rus, and S. Han, “BEVFusion: Multi-Task Multi-Sensor Fusion with Unified Bird’s-Eye View Representation,” in *2023 IEEE International Conference on Robotics and Automation (ICRA)*, May 2023, pp. 2774–2781.
- [66] M. Meyer and G. Kuschk, “Deep Learning Based 3D Object Detection for Automotive Radar and Camera,” in *2019 16th European Radar Conference (EuRAD)*, Oct. 2019, pp. 133–136.
- [67] L. Wang, X. Zhang, B. Xv, J. Zhang, R. Fu, X. Wang, L. Zhu, H. Ren, P. Lu, J. Li, and H. Liu, “InterFusion: Interaction-based 4D Radar and LiDAR Fusion for 3D Object Detection,” in *2022 IEEE/RSJ International Conference on Intelligent Robots and Systems (IROS)*, Oct. 2022, pp. 12 247–12 253.
- [68] J. Giroux, M. Bouchard, and R. Laganiere, “T-FFTRadNet: Object Detection with Swin Vision Transformers from Raw ADC Radar Signals,” Mar. 2023.
- [69] B. Yang, I. Khatri, M. Happold, and C. Chen, “ADCNet: Learning from Raw Radar Data via Distillation,” Dec. 2023.
- [70] T. Boot, N. Cazin, W. Sanberg, and J. Vanschoren, “Efficient-DASH: Automated Radar Neural Network Design Across Tasks and Datasets,” in *2023 IEEE Intelligent Vehicles Symposium (IV)*, Jun. 2023, pp. 1–7.
- [71] Y. Dalbah, J. Lahoud, and H. Cholakkal, “TransRadar: Adaptive-Directional Transformer for Real-Time Multi-View Radar Semantic Segmentation,” in *Proceedings of the IEEE/CVF Winter Conference on Applications of Computer Vision*, 2024, pp. 353–362.
- [72] Y. Jin, A. Deligiannis, J.-C. Fuentes-Michel, and M. Vossiek, “Cross-Modal Supervision-Based Multitask Learning With Automotive Radar Raw Data,” *IEEE Transactions on Intelligent Vehicles*, vol. 8, no. 4, pp. 3012–3025, Apr. 2023.
- [73] Y. Liu, F. Wang, N. Wang, and Z. Zhang, “Echoes Beyond Points: Unleashing the Power of Raw Radar Data in Multi-modality Fusion,” in *Thirty-Seventh Conference on Neural Information Processing Systems*, Nov. 2023.
- [74] D.-H. Paek, S.-H. Kong, and K. T. Wijaya, “Enhanced K-Radar: Optimal Density Reduction to Improve Detection Performance and Accessibility of 4D Radar Tensor-based Object Detection,” in *2023 IEEE Intelligent Vehicles Symposium (IV)*, Jun. 2023, pp. 1–6.
- [75] J. Ku, M. Mozifian, J. Lee, A. Harakeh, and S. L. Waslander, “Joint 3D Proposal Generation and Object Detection from View Aggregation,” in *2022 IEEE/RSJ International Conference on Intelligent Robots and Systems (IROS)*, Oct. 2018, pp. 1–8.
- [76] Y. Yan, Y. Mao, and B. Li, “SECOND: Sparsely Embedded Convolutional Detection,” *Sensors*, vol. 18, no. 10, p. 3337, Oct. 2018.

- [77] X. Weng, J. Wang, D. Held, and K. Kitani, “3D Multi-Object Tracking: A Baseline and New Evaluation Metrics,” in *2020 IEEE/RSJ International Conference on Intelligent Robots and Systems (IROS)*, Oct. 2020, pp. 10359–10366.
- [78] M. L. Puri and C. R. Rao, “Augmenting Shapiro-Wilk Test for Normality,” in *Contribution to Applied Statistics*, W. J. Ziegler, Ed., Basel: Birkhäuser Basel, 1976, vol. 22, pp. 129–139.
- [79] A. Zhang, F. E. Nowruzi, and R. Laganiere, “RADDet: Range-Azimuth-Doppler based Radar Object Detection for Dynamic Road Users,” in *2021 18th Conference on Robots and Vision (CRV)*, vol. 19, May 2021, pp. 95–102.
- [80] A. Valada, R. Mohan, and W. Burgard, “Self-Supervised Model Adaptation for Multimodal Semantic Segmentation,” *International Journal of Computer Vision*, vol. 128, no. 5, pp. 1239–1285, May 2020.
- [81] Y. Zhuang, B. Wang, J. Huai, and M. Li, “4D iRIM: 4D Imaging Radar Inertial Odometry and Mapping,” *IEEE Robotics and Automation Letters*, vol. 8, no. 6, pp. 3246–3253, Jun. 2023.
- [82] Y. Z. Ng, B. Choi, R. Tan, and L. Heng, “Continuous-time Radar-inertial Odometry for Automotive Radars,” Jan. 2022.
- [83] S. Lu, G. Zhuo, L. Xiong, X. Zhu, L. Zheng, Z. He, M. Zhou, X. Lu, and J. Bai, “Efficient Deep-Learning 4D Automotive Radar Odometry Method,” *IEEE Transactions on Intelligent Vehicles*, pp. 1–15, 2023.
- [84] C. Doer and G. F. Trommer, “Radar Visual Inertial Odometry and Radar Thermal Inertial Odometry: Robust Navigation even in Challenging Visual Conditions,” in *Gyroscopy and Navigation*, Sep. 2021, pp. 331–338.
- [85] J. Michalczuk, R. Jung, and S. Weiss, “Tightly-Coupled EKF-Based Radar-Inertial Odometry,” in *2022 IEEE/RSJ International Conference on Intelligent Robots and Systems (IROS)*. Kyoto, Japan: IEEE, Oct. 2022, pp. 12336–12343.
- [86] G. Kim and A. Kim, “Scan Context: Egocentric Spatial Descriptor for Place Recognition Within 3D Point Cloud Map,” in *2018 IEEE/RSJ International Conference on Intelligent Robots and Systems (IROS)*. Madrid: IEEE, Oct. 2018, pp. 4802–4809.
- [87] J. Zhang, H. Zhuge, Z. Wu, G. Peng, M. Wen, Y. Liu, and D. Wang, “4DRadarSLAM: A 4D Imaging Radar SLAM System for Large-scale Environments based on Pose Graph Optimization,” in *2023 IEEE International Conference on Robotics and Automation (ICRA)*, May 2023, pp. 8333–8340.
- [88] C. X. Lu, M. R. U. Saputra, P. Zhao, Y. Almalioglu, P. P. B. de Gusmao, C. Chen, K. Sun, N. Trigoni, and A. Markham, “milliEgo: Single-chip mmWave Radar Aided Egomotion Estimation via Deep Sensor Fusion,” Oct. 2020.
- [89] C. Doer and G. F. Trommer, “An EKF Based Approach to Radar Inertial Odometry,” in *2020 IEEE International Conference on Multisensor Fusion and Integration for Intelligent Systems (MFI)*, Sep. 2020, pp. 152–159.
- [90] X. Li, H. Zhang, and W. Chen, “4D Radar-Based Pose Graph SLAM With Ego-Velocity Pre-Integration Factor,” *IEEE Robotics and Automation Letters*, vol. 8, no. 8, pp. 5124–5131, Aug. 2023.
- [91] A. Galeote-Luque, V. Kubelka, M. Magnusson, J.-R. Ruiz-Sarmiento, and J. Gonzalez-Jimenez, “Doppler-only Single-scan 3D Vehicle Odometry,” Oct. 2023.
- [92] B. Wang, Y. Zhuang, and N. El-Bendary, “4D RADAR/IMU/GNSS INTEGRATED POSITIONING AND MAPPING FOR LARGE-SCALE ENVIRONMENTS,” *The International Archives of the Photogrammetry, Remote Sensing and Spatial Information Sciences*, vol. XLVIII-1/W2-2023, pp. 1223–1228, Dec. 2023.
- [93] J. Zhang, R. Xiao, H. Li, Y. Liu, X. Suo, C. Hong, Z. Lin, and D. Wang, “4DRT-SLAM: Robust SLAM in Smoke Environments using 4D Radar and Thermal Camera based on Dense Deep Learnt Features,” in *10th IEEE International Conference on Cybernetics and Intelligent Systems (CIS) and the 10th IEEE International Conference on Robotics, Automation and Mechatronics (RAM)*, Jun. 2023.
- [94] H. Chen, Y. Liu, and Y. Cheng, “DRO: Robust Radar-Inertial Odometry in Dynamic Environments,” *IEEE Robotics and Automation Letters*, vol. 8, no. 9, pp. 5918–5925, Sep. 2023.
- [95] G. Zhuo, S. Lu, H. Zhou, L. Zheng, and L. Xiong, “4DRVO-Net: Deep 4D Radar-Visual Odometry Using Multi-Modal and Multi-Scale Adaptive Fusion,” Aug. 2023.
- [96] C. Doer and G. F. Trommer, “Yaw aided Radar Inertial Odometry using Manhattan World Assumptions,” in *2021 28th Saint Petersburg International Conference on Integrated Navigation Systems (ICINS)*, May 2021, pp. 1–9.
- [97] ——, “X-RIO: Radar Inertial Odometry with Multiple Radar Sensors and Yaw Aiding,” *Gyroscopy and Navigation*, vol. 12, no. 4, pp. 329–339, Dec. 2021.
- [98] C. Doer, J. Atman, and G. F. Trummer, “GNSS aided Radar Inertial Odometry for UAS Flights in Challenging Conditions,” in *2022 IEEE Aerospace Conference (AERO)*, Mar. 2022, pp. 1–10.
- [99] H. W. Kuhn, “The Hungarian method for the assignment problem,” *Naval Research Logistics Quarterly*, vol. 2, no. 1-2, pp. 83–97, Mar. 1955.
- [100] K. Koide, J. Miura, E. Menegatti, H.-W. Cho, W. Kim, S. Choi, M. Eo, S. Khang, and J. Kim, “A portable three-dimensional LIDAR-based system for long-term and wide-area people behavior measurement,” *International Journal of Advanced Robotic Systems*, vol. 16, no. 2, p. 172988141984153, Mar. 2019.
- [101] A. Segal, D. Haehnel, and S. Thrun, “Generalized-ICP,” in *Robotics: Science and Systems V*, vol. 2. Seattle, WA, 2009, p. 435.
- [102] P. Biber and W. Strasser, “The normal distributions transform: A new approach to laser scan matching,” in *Proceedings 2003 IEEE/RSJ International Conference on Intelligent Robots and Systems (IROS 2003) (Cat. No.03CH37453)*, vol. 3. Las Vegas, Nevada, USA: IEEE, 2003, pp. 2743–2748.



Zeyu Han received the bachelor’s degree in automotive engineering from School of Vehicle and Mobility, Tsinghua University, Beijing, China, in 2021. He is currently pursuing the Ph.D. degree in mechanical engineering with School of Vehicle and Mobility, Tsinghua University, Beijing, China. His research interests includes autonomous driving SLAM and environment understanding by 4D mmWave radars.



Jiahao Wang earned the Bachelor’s degree in Automotive Engineering from the School of Vehicle and Mobility at Tsinghua University, Beijing, China, in 2022. He is presently pursuing the Ph.D. degree in Mechanical Engineering at the same institution. His current research is centered on scene comprehension and robust multimodal 3D perception for autonomous driving.



Zikun Xu earned his bachelor’s degree in measurement and control technology and instruments from the School of Mechanical, Electronic and Control Engineering, Beijing Jiaotong University, Beijing, China, in 2023. He is currently pursuing his Ph.D. degree in mechanical engineering with the School of Vehicle and Mobility, Tsinghua University, Beijing 100084, China. His research interests include drivable area detection and scene understanding.



Shuocheng Yang is currently pursuing a bachelor’s degree in Theoretical and Applied Mechanics and Vehicle Engineering at Tsinghua University’s Xingjian College. His research focuses on radar-based SLAM.



Lei He received his B.S. in Beijing University of Aeronautics and Astronautics, China, in 2013, and the Ph.D. in the National Laboratory of Pattern Recognition, Chinese Academy of Sciences, in 2018. From then to 2021, Dr. He served as a postdoctoral fellow in the Department of Automation, Tsinghua University, Beijing, China. He worked as the research leader of the Autonomous Driving algorithm at Baidu and NIO from 2018 to 2023. He is a Research Scientist in automotive engineering with Tsinghua University. His research interests include Perception, SLAM, Planning, and Control.



Shaobing Xu received his Ph.D. degree in Mechanical Engineering from Tsinghua University, Beijing, China, in 2016. He is currently an assistant professor with the School of Vehicle and Mobility at Tsinghua University, Beijing, China. He was an assistant research scientist and postdoctoral researcher with the Department of Mechanical Engineering and Mcity at the University of Michigan, Ann Arbor. His research focuses on vehicle motion control, decision making, and path planning for autonomous vehicles. He was a recipient of the outstanding Ph.D. dissertation award of Tsinghua University and the Best Paper Award of AVEC'2018.



Jianqiang Wang received the B. Tech. and M.S. degrees from Jilin University of Technology, Changchun, China, in 1994 and 1997, respectively, and Ph.D. degree from Jilin University, Changchun, in 2002. He is currently a Professor of School of Vehicle and Mobility, Tsinghua University, Beijing, China. He has authored over 150 papers and is a co-inventor of over 140 patent applications. He was involved in over 10 sponsored projects. His active research interests include intelligent vehicles, driving assistance systems, and driver behavior. He was a recipient of the Best Paper Award in the 2014 IEEE Intelligent Vehicle Symposium, the Best Paper Award in the 14th ITS Asia Pacific Forum, the Best Paper Award in 2017 IEEE Intelligent Vehicle Symposium, the Changjiang Scholar Program Professor in 2017, Distinguished Young Scientists of NSF China in 2016, and New Century Excellent Talents in 2008.



Keqiang Li received the B.Tech. degree from Tsinghua University of China, Beijing, China, in 1985, and the M.S. and Ph.D. degrees in mechanical engineering from the Chongqing University of China, Chongqing, China, in 1988 and 1995, respectively. He is currently a Professor with the School of Vehicle and Mobility, Tsinghua University. His main research areas include automotive control system, driver assistance system, and networked dynamics and control, and is leading the national key project on CAVs (Connected and Automated Vehicles) in China. Dr. Li has authored more than 200 papers and is co-inventor of over 80 patents in China and Japan. Dr. Li has served as a Fellow Member of Chinese Academy of Engineering, a Fellow Member of Society of Automotive Engineers of China, editorial boards of the International Journal of Vehicle Autonomous Systems, Chairperson of Expert Committee of the China Industrial Technology Innovation Strategic Alliance for CAVs (CACAV), and CTO of China CAV Research Institute Company Ltd. (CCAV). He has been a recipient of Changjiang Scholar Program Professor, National Award for Technological Invention in China, etc.